

An-Najah National University

Faculty of Graduate Studies

**Sustainable Power Solution by Monolithic Integrated
PV-Battery**

By

Mohammed Walid Mohammed Jaber

Supervisor

Dr. Tamer Khatib

**This Thesis is Submitted in Partial Fulfillment of the Requirements for
the Degree of Master of Clean Energy Conservation Engineering,
Faculty of Graduate Studies, An-Najah National University,
Nablus - Palestine.**

2019

Sustainable Power Solution by Monolithic Integrated PV-Battery

By

Mohammed Walid Mohammed Jaber

This thesis was defended successfully on / / and approved by:

Defense Committee Members

Signature

- **Dr. Tamer Khatib / Supervisor**
- **Dr. Dhiaa Muhsen / External Examiner**
- **Dr. Iyad Saadeddin / Internal Examiner**

Dedication

"I dedicate my achievement to my family and my friends. A special feeling of gratitude to my loving parents, Waleed, and Eman whose words of encouragement and push for tenacity ring in my ears, and to the teachers who never left my side.

I also dedicate this work to many friends who have supported me throughout the process, and not to forget the late-night caffeine's cups which kept me awake for long hours and brought me to this success."

Acknowledgment

“He who does not thank the people is not thankful to God”

Prophet Mohammed

Give all thanks and appreciation to *Device development* group in *IEK-5* at *Forschungszentrum Jülich, Germany* whose did not hesitate to support me at all stage of the project.

الإقرار

أنا الموقع أدناه مقدم الرسالة التي تحمل العنوان:

Sustainable Power Solution by Monolithic Integrated PV-Battery

أقر بأن ما اشتملت عليه هذه الرسالة هو نتاج جهدي الخاص، باستثناء ما تمت الإشارة إليه حيث ورد، وأن هذه الرسالة ككل أو أي جزء منها لم يقدم من قبل لنيل أي درجة أو لقب علمي أو بحثي لدى أي مؤسسة تعليمية أو بحثية أخرى.

Declaration

The work provided in this thesis, unless otherwise referenced, is the researcher's own work, and has not been submitted elsewhere for any other degrees or certifications.

Student's Name:

إسم الطالب:

Signature:

التوقيع:

Date:

التاريخ

Table of Content

No	Content	Pages
	Dedication	Iii
	Acknowledgment	Iv
	Declaration	V
	List of Tables	Vii
	List of Figures	Viii
	Abstract	Xi
	Chapter One: Introduction	1
1.1	Background	1
1.2	Problem statement	3
1.3	Research Objectives	3
1.4	Organization of thesis	4
	Chapter Two: Methodology	6
2.1	Structure and preparation of 2T and 3T solar cell	6
2.2	Light sources and spectra	15
2.3	Different illumination intensity and spectrum dependent performance of solar cell	18
	Chapter Three: Experiments	20
3.1	Optical measurements (UV-VIS spectroscopy measurements)	20
3.2	Current-voltage measurements	22
3.3	Differential spectral response (DSR) measurements	25
3.4	Charge/Discharge analysis of 3T solar cell and battery	26
	Chapter Four: Result and discussions	29
4.1	Development and optimization 3T device	29
4.2	The electrical loss in parallel mode	36
4.3	Optical loss analysis	37
4.4	Dependence of PV parameters on Illumination intensity and spectra for 3 T triple-junction solar cells	39
4.5	Comparison between 2T and 3T triple-junction solar cells	44
4.6	Comparison between 3T, SHJ, and Perovskite solar cell	46
4.7	The performance of integrated three-terminal/triple-junction thin-film module and a lithium Ion battery	49
	Chapter five Conclusion and Future Work	52
	References	54
	المخلص	ب

VII
List of Tables

No	Title	Pages
Table 2. 1	Deposition parameters of a-Si:H and $\mu\text{c-Si:H}$.	13
Table 3. 1	Deposition parameter for ten single-junction cells based on (a-Si) and ($\mu\text{c-Si}$). Current-voltage measurements	22
Table 4. 1	PV parameter of 3T-device, sample (17L-312-3), cell 10, under AM1.5 illumination	32
Table 4. 2	PV parameter of 3T-device, samples (18L-203-2, 18L-197-2), cell 10, 09 respectively under AM1.5 illumination	35
Table 4. 3	Electrical losses in parallel mode	37
Table 4. 4	Efficiencies for 3T-device and 2T triple junction solar cells and single-junction a-Si:H and $\mu\text{c-Si:H}$ solar cells	42
Table 4. 5	Current density (JSC) for 3T-device and 2T triple-junction solar cells and single-junction a-Si:H and $\mu\text{c-Si:H}$ solar cells in (mA/cm ²) unit	42
Table 4. 6	IV Parameters of the module	50

VIII
List of Figures

No.	Title	Page
Figure 1.1	Organization of thesis	5
Figure 2. 1	PECVD system [6]	9
Figure 2. 2	Sketch of the single junction solar cell of (a) a-Si and (b) $\mu\text{c-Si:H}$ [7]	9
Figure 2. 3	Tandem solar cell based on a-Si:H/ $\mu\text{c-Si:H}$ in 2-terminal configuration	11
Figure 2. 4	Three terminal/triple-junction thin film solar cell [7]	14
Figure 2. 5	Spectrum response for AM1.5g in black line and AM1.5 from solar simulator in blue line	16
Figure 2. 6	Wacom Solar Simulator WXS-90S-L2 AM1.5GMMKeithley SMU Models 2612B System Source Meter Instruments from Tektronix Company [8]	17
Figure 2. 7	Spectrum response for LED, Halogen, fluorescent light sources	17
Figure 2. 8	Normalized spectral irradiation for different filters	19
Figure 3. 1	LAMBDA 950 UV/Vis Spectrophotometer.[10]	21
Figure 3. 2	Schematic circuit for load switching	23
Figure 3. 3	Equivalent circuit for the solar cell	24
Figure 3. 4	IV-curve of an ideal solar cell	25
Figure 3. 5	QE monochromator-based setup	26
Figure 3. 7	ICP501230PS-03 Rechargeable Lithium Ion Polymer Battery Pack 3.7 V	27
Figure 3. 8	Charge/discharge circuit, current and voltage sense, and battery connected directly with a solar cell. [13]	28
Figure 4. 1	sample number 17L-312-3 (a) top view of the whole sample (b) order of subcell connections	30
Figure 4. 2	Schematic drawing of 3T-device and diode structure	30
Figure 4. 3	IV-characteristics for a-Si:H top sub cell, $\mu\text{c-Si:H}/\mu\text{c-Si.H}$ bottom tandem sub cell, and the a-Si:H/ $\mu\text{c-Si:H}/\mu\text{c-Si:H}$ cell from sample (17L-312-3)	31

Figure 4. 4	External Quantum Efficiency of sample number (17L-312-3)	33
Figure 4. 5	IV-characteristic curve (a) sample number (18L-203-2) (b) sample number (18L-197-2)	34
Figure 4. 6	External Quantum Efficiency of 3T-device, the continuous line represent sample number (18L-197-2) cell number (09), and the dashed line represent sample number (18-203-2) cell number (10)	35
Figure 4. 7	scheme for configuration of 3T-device and PV-parameters for each subcell for sample number (18L-197-2) cell number (09)	36
Figure 4. 8	Schematic drawing of 3T-device	37
Figure 4. 9	Absorption spectra for a-Si:H single junction cells with different back contact and different thickness of the n-layers	38
Figure 4. 10	Open-circuit voltage ((a)-(d)) and fill factor ((f)-(i)) for 3T-device measured in parallel mode (black square, total cell) and separate mode (green circle and blue triangle represent top and bottom tandem subcell, respectively)	40
Figure 4. 11	Spectral irradiation for different filters	41
Figure 4. 12	Efficiencies of (a) 3T device based on triple junction solar cell in parallel mode (b) a-Si:H top and $\mu\text{c-Si:H}/\mu\text{c-Si:H}$ tandem- subcells in separate mode (c) single-junction a-Si:H and $\mu\text{c-Si:H}$ solar cells [14] under different light sources.	43
Figure 4. 13	Comparison between 3T- and 2T-device based on triple junction a-Si:H/ $\mu\text{c-Si:H}/\mu\text{c-Si:H}$ under different light sources (a) efficiency (b) open-circuit voltage (c) fill factor	45
Figure 4. 14	Schematic drawing of (a) Perovskite (b) SHJ solar cells	46
Figure 4. 15	Comparison of PV parameters (a) efficiency (b) open-circuit voltage (c) fill factor for 3T-device, Perovskite, and SHJ as a function of J_{sc} for different light sources	47

Figure 4. 16	Normalized spectral irradiance of the different light sources used for this study in comparison with the normalized external quantum efficiency (EQE) of perovskite and SHJ solar cells	48
Figure 4. 17	Normalized spectral irradiance of the different light sources used for this study in comparison with the normalized external quantum efficiency (EQE) of 3T-device subcells	49
Figure 4. 18	Characteristic of 3T-device under AM1.5 illumination (a)IV curve for one cell from the module (b) IV curve for five cells connected in series.	50
Figure 4. 19	Charge/Discharge profile for 3T-device with (3.7V, 135mAh) battery	51

Sustainable Power Solution by Monolithic Integrated PV-Battery**By****Mohammed Walid Mohammed Jaber****Supervisor****Dr. Tamer Khatib****Abstract**

The global energy crisis and energy conservation for sustainability the most concern of the scientific community and solar energy is one of the leading solutions to this crisis. Improve the efficiency of solar cells and energy storage systems the most important topics, where efficiency record of (26.6%) of *c-Si* solar cells. Also find an efficient energy storage system from solar cells ensure provided energy at times of absence of a light source. Solid-state battery most common component used to store and reuse electrical energy. By combining these two systems (high efficient solar cells and solid-state battery) to get integrated photovoltaic-battery (PV-battery) will be founded a sustainable solution. This study will review the accurate description for design stages of the PV part of the proposed Integrated system and design three terminal/triple-junction solar cell (3T-device). Deposit multi-junction TFSC composed from amorphous (a-Si:H) as top subcell, and microcrystalline ($\mu\text{c-Si:H}/\mu\text{c-Si:H}$) as bottom tandem subcell, with (p-i-n/n-i-p/n-i-p) configuration respectively, through PECVD technology. Upgraded 2T-device which had deposited to 3T-device to solve mismatching current problem by inserting new terminal between the top and bottom tandem subcell. Also, developed voltage of 3T-device to

solve mismatching voltage occur between the top and bottom tandem subcell. As a result of that, has been achieved matching voltage reach to 95.67% (0.853, 0.816, 0.841 V, top, bottom, and total cell respectively). In addition, spectral response for 3T-device under different light sources (AM1.5, LED, fluorescent-tube, halogen), and different levels of light intensity (1sun to 0.0000194sun) had been studied. Measure and analysis of cell parameters (V_{OC} , I_{SC} , FF, η) as a function of current intensity (J_{SC}) shown 16.4% efficiency under LED light source. likewise, analysis parameters of 2T-device, Perovskite, and SHJ under different light sources and light intensity to hold comparison between them with 3T-device. Clearly shown good performance of perovskite under LED and SHJ under AM1.5 which recorded efficiency reach about 29% and 15.4% respectively. Studied behavior of light beam through window cell and determination of the parameters causing the optical losses shown the main effect of a (ZnO/Ag/ZnO) as back contact of top subcell. In the final stage, check the ability of 3T-device to charging of a commercial battery model (135mAh, 3.7V) which recorded solar energy to charge conversion efficiency around (10%) under (AM1.5) light source.

Chapter One

Introduction

1.1 Background

The world is alerted to the need for alternative energy sources after the 1973 oil 'shock', which has a considerable effect on the economy [1]. Moreover, the balance between energy supply and demand has become an important issue over time due to the continuous increase in the population. By 2015, the total final world consumption (TFC) reached to (376 EJ) [2], while for the same year, above (87.5 EJ) total energy production was recorded for electrical energy [3].

Renewable energy is created by harnessing and replenishing the earth's natural resources such as wind and solar energy. These sources will never run out and constantly available. Moreover, it is clean energy and environmentally friendly in contrast to the non-renewable sources like crude oil, natural gas, coal, and nuclear source, which causes a global warming and air pollution. Therefore, it is the promising, sustainable and clean solution for the world energy crisis.

With trends of electrical consumption which is increasing over years, and continuous decrease in the fossil fuel sources, (12.1%) renewable energy used in power generation from 2007 to 2017 [4]. This percentage is considered to be little comparing to the contribution of non-renewable source. Therefore, the world is looking to increase the contribution of a renewable source to (25%) by 2030 to harvest more benefits.

Particularly intriguing is the solar energy which has become among the fastest growing class of renewable energy source. This energy type is attractive from point of view for prospective applications, e.g. solar powered water pump and solar panel. The solar panel is composed of many solar modules which are typical examples of photovoltaic (PV) devices, each converts the sunlight energy into an electrical power. When semiconductors materials like silicon (Si) exposure to sunlight, the photon which has energy equal or greater than the energy of band gap (E_g) will excited electrons to move. While electric leaving its position from the valence band leave behind its hole. Those electrons (e) and holes (h) called negative and positive carriers respectively. The carriers (e/h) moves and collected from electrodes. In the last two decades, the efficiency of the solar cell significantly increased, and that refers to the improvement of the semiconductor properties like light trapping and collecting surface area minimization. Furthermore, the source of semiconductor materials is abundant and easy to compose and manufacture. The most common PV systems are Silicon (*Si*)-based.

The thin-film silicon solar cell (TFSC) technology is a vision to produce solar cell on glass in a thickness less than the thickness of silicon solar cell which is (200) μm . With TFSC technology, the thickness of the whole solar cell reaches to (1-2) μm , On the other hand, the thinner cell can also lead to lowering materials consumption, leading to low production cost and minimizing the energy payback time. All these factors can play a key role

to make and support TFSC to be feasible and competitive on the industrial scale.

1.2 Problem statement

Besides, the battery is the most common kind of storage system which converts the electrical energy that is generated from PV to a chemical energy. It has been used in low consumption devices like smartphones, calculators, watches...etc. However, such battery has to be replaced with new one or has to be recharged from the grid, and the main challenge lies in the availability of the grid, in particular for the more critical applications which serve the human health and safety like medical monitoring and emergency sign. In addition, there is an environmental impact upon batteries disposal. To overcome these problems, we have to *combine the batteries of the devices with an alternative power source*.

All these indicators point on a sustainable solution that can provide applicable device consist of an energy source and storage system with maximum possible overall efficiency(η), and economically visible.

1.3 Research Objectives

The aims of this work are to study the performance of 3 terminals versus 2 terminal thin film silicon devices as a function of different light intensity and spectra. Additionally, the influences of various light intensities and spectra on the IV parameters of highly performance

perovskite and silicon heterojunction solar cells (SHJ) were investigated. At the end we aim integration between PV-battery.

Besides, to test more types of batteries and to get more efficient solar cell include using charge control electronics.

1.4 Organization of thesis

In order to achieve these aims, three-terminal (3T) solar cell device preparation was the first step, then studying its behavior under different illumination intensities, these will be shown in Chapter 2. Later on, the utilized characterization methods for studying 3T solar cell device will be outlined in Chapter 3. The obtained results will be shown and discussed in Chapter 4. Furthermore, a comparison between (two-terminal) 2T and 3T solar cell device and another comparison between 3T and silicon heterojunction (SHJ) and perovskite solar cell as well will be addressed. For the integration, the obtained PV-battery as a system will be also shown. Finally, the summary and outlook which will give the recommendation and further possibility of modifications and improvements will be presented in Chapter 5.



Figure 2.1: Organization of thesis

Chapter Two

Methodology

2.1 Structure and preparation of 2T and 3T solar cell

Silicon (*Si*) is the most used semiconductor material, with atomic number (14). Of these, four are valence electrons which are shared, forming covalent bonds with the four surrounding (*Si*) atoms and a pattern of crystalline silicon (*c-Si*) matrix is configured in a tetrahedron structure. Both the bond angle and bond length influence the order of crystalline silicon, when they vary, a disturbance in the ordering state is introduced and amorphous (*Si*) (*a-Si*) is formed. For (*a-Si*) thin films, the value of bond angle deviated between (6° to 9°) from the fixed value for monocrystalline silicon wafers which is ($109^\circ 28'$). The dominated crystal structure in (*a-Si*) is a random pattern for bond angle and length. [5]

Furthermore, due to randomness, many of bonds are lost, these called "dangling bonds", and they will break due to emitted energy from recombining close to the bond, and that called light-induced degradation effect or *Staebler-Wronski effect (SWE)*. After breaking the bond, a hydrogen atom (*H*) builds a covalent bond with the silicon atom (*Si*), most of the broken bonds are paired with a hydrogen atom, therefore a hydrogenated amorphous silicon (*a-Si:H*) is formed.

Hydrogenated microcrystalline silicon (*μc -Si:H*) is another type of material that can be used in thin-film technology, "Microcrystalline" refers

to "conglomerates" which are composed of "grains", and they have a dimension of about (1 μm). The conglomerates play a key role in improving the collection properties for ($\mu\text{c-Si:H}$) with less thickness. ($\mu\text{c-Si:H}$) contains both amorphous and crystalline phases which are controlled by the hydrogen dilution ratio $R=[\text{H}_2]/[\text{SiH}_4]$ during thin film deposition. The deposition process, more crystallinity can be achieved by increasing R , therefore, with tuning R one can produce many types of ($\mu\text{c-Si:H}$).

The electrical properties of silicon can be modulated, by doping it with an element from *group V* such as *P, As, Sb* or element from *group III* e.g. *B, Ga, In, Al*. The doping percentage depends on the required charge carrier's concentration (electrons and holes). When doping (Si) with an element from *group V*, which has five valence electrons, four of these electrons will form covalent bonds with (Si) atoms. The extra 5th electron will be located in an energy state (donor energy state) that is located at the immediate vicinity of the conduction band. The electron is thermally excited and becomes free in the conduction band. The temperature needed to excited electron is very low (about 50^o K). Hence at room temperature, almost all extra electrons from donor atoms are excited to the conduction band. Since the electron has a negative charge then the process is called n-doping to introduce n-type semiconductor (n-type Si). On another hand, when using an element from *group III* which has three valence electrons, all these electrons will form covalent bonds with Si atoms. The deficient electrons (called "hole") will be located in an energy state (acceptor energy state) that is located at the valence band. Since hole has a positive charge

then the process is called p-doping to introduce p-type semiconductor (p-type Si). Thus, by doping semiconductor material, one can create *p*- and *n*-layers for the thin film solar cell (*i*-layer means intrinsic silicon without any foreign atoms).

The Plasma-enhanced chemical vapor deposition (PECVD) method is used to prepare thin film solar cells. It is a chemical vapor deposition process to deposit thin films from vapor to a solid state on a substrate via plasma rather than high temperature. The below schematics (Figure 2.1) show PECVD equipment. Deposition of thin-films by PECVD are summarized by the following steps:

1. Pumping chamber down (making vacuum) to provide a clean environment for deposition.
2. Flow target gas to the chamber. Silane (SiH_4) was used as a source gas in a PECVD process, the electron impact processes lead to reactive neutral species such as SiH , SiH_2 , SiH_3 , Si_2H_6 , H and H_2 and ionized species such as SiH^+ , SiH_2^+ , SiH_3^+ .
3. Applied RF voltage to the electrodes of the chamber to ionize the gas molecules. This ionization process makes the molecules of the source gas chemically reactive and then these molecules form a thin layer of material on our substrate.
4. The thickness of layers growth with time.

5. Pumped the chamber down again to remove all of the gases and products of the deposition process.

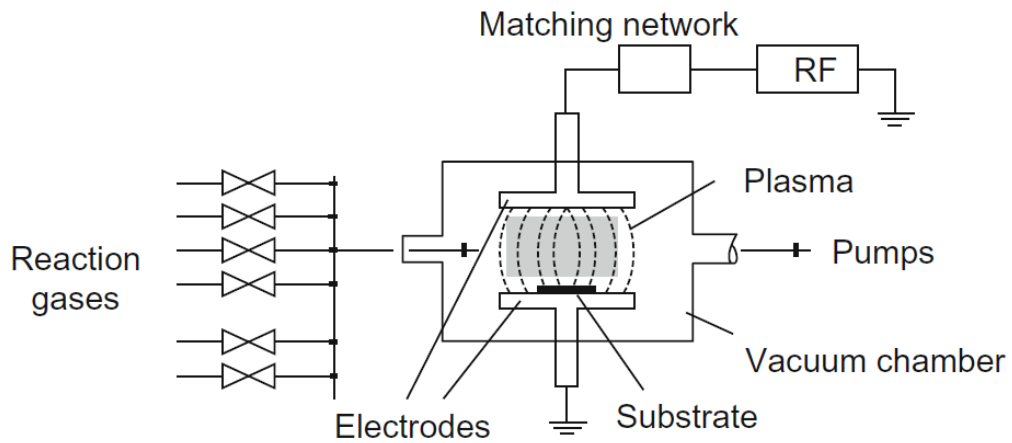


Figure 2. 1: PECVD system [6]

After the deposition process is finished, the following structure for a-Si:H and $\mu\text{c-Si:H}$ (Figure 2.2) will be obtained:

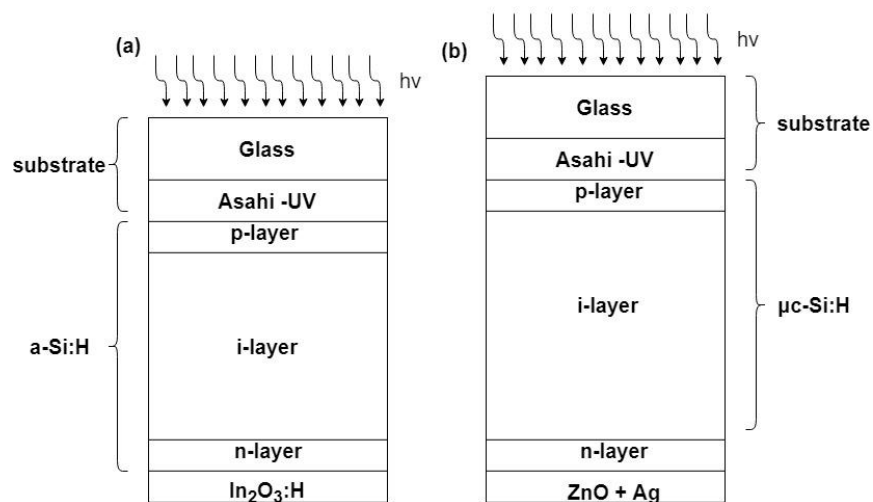


Figure 2. 2: Sketch of the single junction solar cell of (a) a-Si and (b) $\mu\text{c-Si:H}$ [7]

In figure 2.2 (a), the structure of hydrogenated amorphous silicon ($a\text{-Si:H}$) is shown. With ($p\text{-i-n}$) structure of very thin p - and n -type layers. Very thin layer is used because ($a\text{-Si:H}$) has a very high density of recombination centers, that leads to increasing recombination rate, therefore loss of carriers. Besides that, using intrinsic layer can be created internal electric field assists to separate electrons and holes and collecting them from n - and p -layers. Regarding amorphous silicon thin films, observed degradation in efficiency after exposure it to illumination to around (1000h) because of *Staebler-Wronski effect (SWE)* which was mentioned previously. Decreasing thickness of the cell and increasing the deposition temperature and dilution ratio (R) during *PECVD* deposition can result in reduction of the SWE.

On right hand of figure 2.2 (b), *Microcrystalline silicon thin films ($\mu\text{c-Si:H}$)* solar cell has ($p\text{-i-n}$) structure like ($a\text{-Si:H}$), but with thick i -layer of about $1\mu\text{m}$. The single-junction ($\mu\text{c-Si:H}$) solar cell are not industrially preferable, but they are used as a bottom cell like tandem solar cells ($a\text{-Si:H}/\mu\text{c-Si:H}$) in 2-terminal configuration. Which composed of two cells, the top layer is amorphous with (1.75 eV) band gap energy and ($p\text{-i-n}$) configuration. The bottom layer is microcrystalline with (1.1 eV) band gap energy and ($p\text{-i-n}$) configuration. Through this combination the cell can absorb visible range and infrared range of sunlight respectively.

Figure 2.3 shows the 2-terminal configuration of tandem cells, the top subcell exposed to *light-induced degradation*. Therefore, the thickness should be thinner as possible. In contrast, decreasing subcell thickness leads to decreasing amount of light absorbed. This can be corrected by using an intermediate reflector (*IR*) between subcells, to reflect the short-wavelength light back into amorphous solar cell.

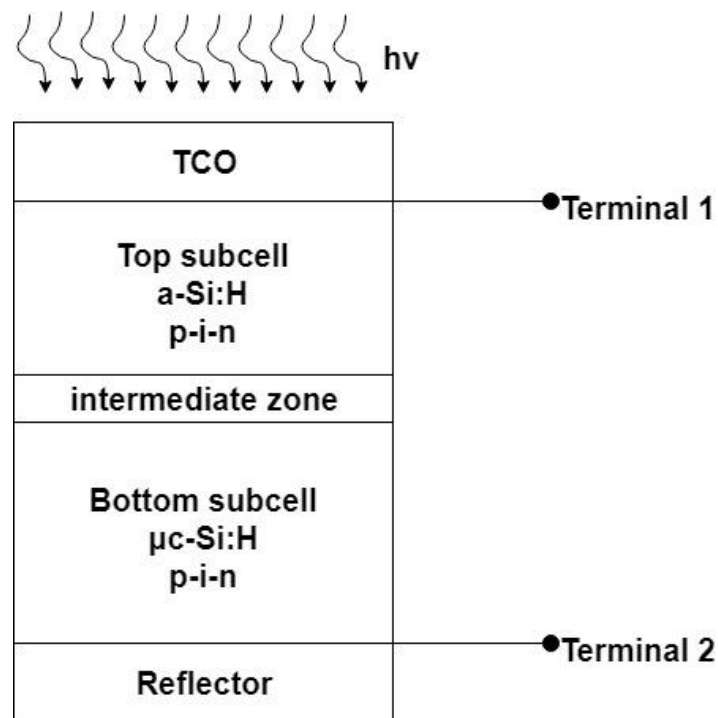


Figure 2. 3: Tandem solar cell based on a-Si:H/μc-Si:H in 2-terminal configuration

When sunlight enters the top cell of micromorph tandem solar cell, the carriers began to moving. The aim of the two terminals shown in figure 2.3 is to collect these carriers. The total current collected by two terminal (*2T*) configurations will be equal to the current generated by each subcell, and the voltage will be the summation voltage of two subcells. The Micromorph tandem solar cells can be considered as two voltage sources

connected in series, so in this configuration, the total current is limited by the lower current. So, the "mismatch current" state is most critical issues to care about it in micromorph tandem cells. The current limitation meaning loss in total power output from cell, the solar cell efficiency decreases.

To avoid the requirements for current matching in 2T configuration here we suggest including third terminal between subcells. This is so called (3T) configuration where the total current will be equal to sum current from two subcells, and voltage will be equal to the voltage of each subcell.

Three terminal (3T)/tandem cell cannot completely solve mismatching problem but transfer it from current to voltage matching requirements. It is easier to match the voltage rather than the current. The schematic drawing of single-junction amorphous silicon (*a-Si:H*) and microcrystalline silicon (*μ c-Si:H*) solar cells is shown in figure 2.2. The layer stacks are deposited by *PECVD* on *ASAHI-VU* glass textured substrate. The following table 2.1 shows deposition parameters.

Table 2. 2 Deposition parameters of a-Si:H and μ c-Si:H.

Cell type & structure		Deposition Parameters						
Subcell	layer	Power [W]	Pressure [Torr]	Temp. [°C]	Frequency [MHz]	Dilution Ratio (R)	Time [sec]	Back contact
<i>a-Si:H</i>	p	45	3	220	13.56	6	75	IO:H
	i-i	25	3	200	13.56	30,5	2400,275	
	n	30	3	220	13.56	6	150	
<i>μc-Si:H</i>	p	450	10	220	13.56	266	120	ZnO+Ag
	i	400	8	160	13.56	80	3000	
	n	30	3	220	13.56	6	150	

The most important issues when composed micromorph tandem cell is "*mismatch voltage*", given the voltages from amorphous V_{OC} : (0.866 V) is two times larger than the voltage of microcrystalline V_{OC} : (0.481 V). To fill gap in voltage, will have to upgrade the number of junctions from tandem- to triple-junction by using another stake from microcrystalline in series mode in bottom subcell, to create three terminal/triple-junction thin film solar cell which called 3T-device, in figure 2.4 sketch of the 3T-device:

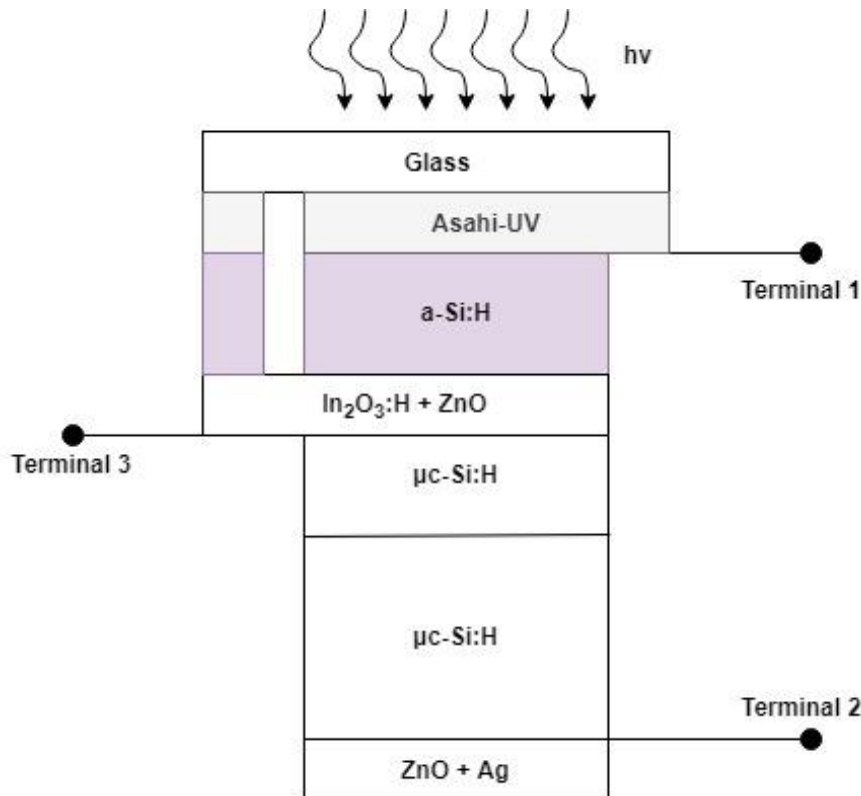


Figure 2. 4: Three terminal/triple-junction thin film solar cell [7]

The first sample (17L-312-3) was deposited in the deposition lab (IEK 5, FJZ) with 3T-device configuration for this study. *ASAHI-VU* Substrate was used, with thickness: (1,8mm). *a-Si* (*p-i-n*) deposited for (50 minutes)

as a top subcell and tandem $\mu c\text{-Si}$ ($n\text{-i-p}/n\text{-i-p}$) deposited for (58) and (111) minutes respectively as a tandem bottom subcell. The intermediate contact between the top and the tandem bottom subcell deposited through two stage. First one with Indium oxide ($In_2O_3:H$), and the second with Zinc oxide (ZnO), and used (ZnO) and Silver (Ag) as back contact.

2.2 Light sources and spectra

The integrated PV-battery can utilize an indoor light source like Light-Emitting Diode (LED), Compact Fluorescent Lamp-tube (CFL), and the Halogen lamp, beside solar radiation ($AM1.5G$). It known that each light source has own spectral response at the same lux level. On the other hand, the solar cells have also spectral response, so the behavior of the solar cell depends on the kind of light source.

Energy harvesting from different light source depends on the spectrum of the light source and the distance between cell and light source. Figure 2.5 shows spectral response for global solar radiation ($AM1.5g$) which contains (1000 W/m^2) as light energy for terrestrial applications, In case $AM1.5g$ is not available to test the cells, we need to simulate natural sunlight by using solar simulator figure 2.5 shows the spectrum irradiation for global natural sunlight spectrum and artificial light from the solar simulator, the wavelength range of artificial light limited to (1100 nm), but the natural sunlight extended to (4000 nm).

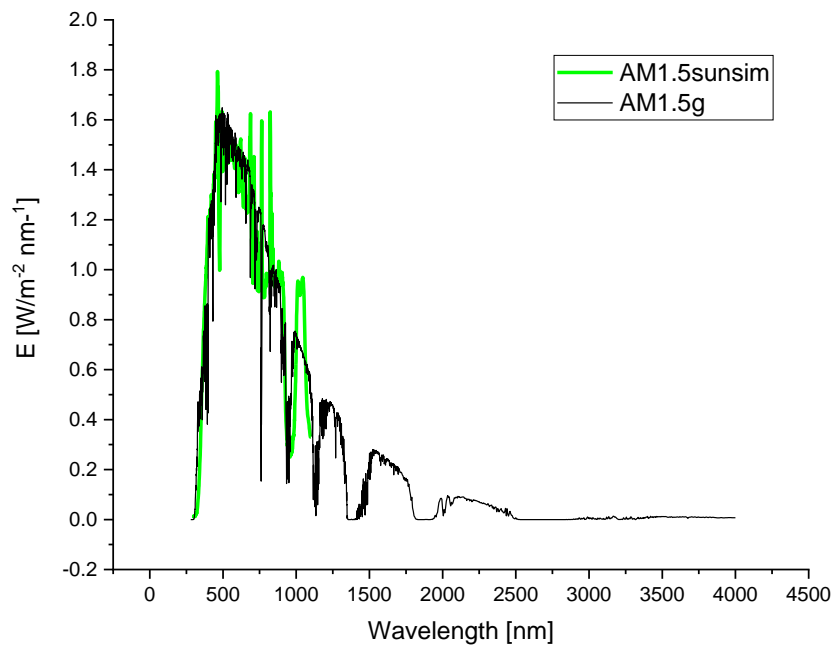


Figure 2. 5: Spectrum response for AM1.5g in black line and AM1.5 from solar simulator in blue line

In our study, we will use the Wacom Solar Simulator WXS-90S-L2 AM1.5GMM which is shown in figure 2.6 from Voss electronic GmbH company. The solar simulator consists of 500W WACOM Xenon and 400W Halogen Lamps. The cell sizes: 100mm x 100mm, Class "AAA" (spectral match class "A": 0.75–1.25, spatial non-uniformity class "A": 2%, temporal instability class "A": 2%) according ASTM standards and measurement unit.



Figure 2. 6: Wacom Solar Simulator WXS-90S-L2 AM1.5GMM Keithley SMU Models 2612B System Source Meter Instruments from Tektronix Company [8]

The indoor light source, which will be used in this study, we choose PARATHOM as a LED light source from OSRAM GmbH, with 3.5W, and 4000K cool white color temperature. A Fluorescent Lamp Standard, NL-T5 4W/25, and color temperature: (4000 K). A Halogen Standard Lamp RJH-A 30W/230/C/XE/E27, with color temperature: (2700 K). Figure 2.7 shows spectral response for each light source respectively.

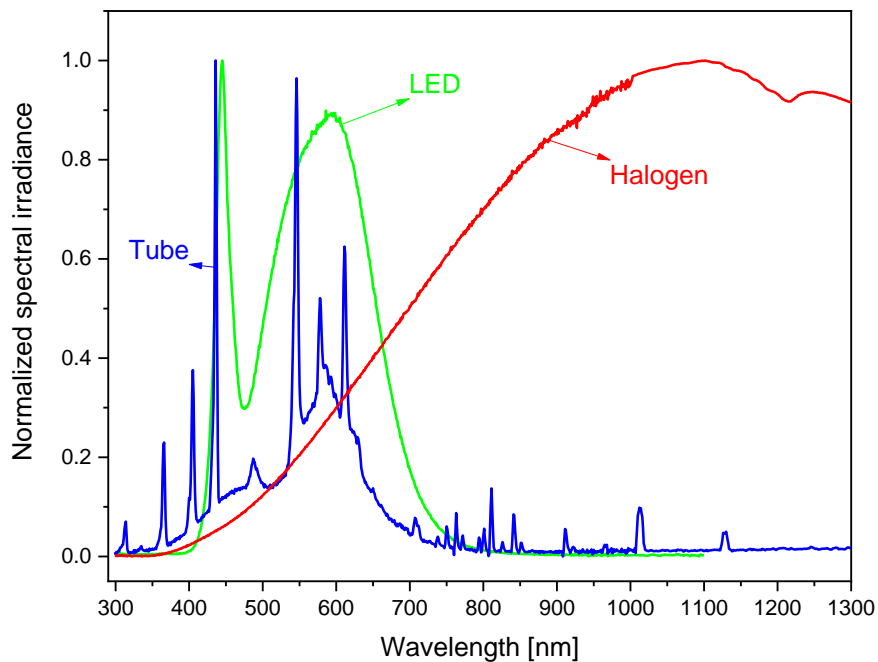


Figure 2. 7: Spectrum response for LED, Halogen, fluorescent light sources.

2.3 Different illumination intensity and spectrum dependent performance of solar cell

Variation of light intensity is a normal phenomenon for light source due to many factors, including shadowing, reflection, distance, and weather. Since the PV-battery device will operate indoor and outdoor. Therefore, studying the illumination intensity behavior of solar cell device is of an importance.

Current-voltage curve (IV-curve), is the most common method to evaluate the performance of the solar cell. The parameters which describe IV-curve are: open-circuit voltage (V_{oc}), short-circuit current (I_{sc}), fill-factor (FF), series resistance (R_s), shunt resistance (R_{sh}), power at maximum power point (P_{mpp}), and efficiency (η). The solar cell parameter are affected by light intensity as reported in the literature. [9] To describe light intensity we usually use (1 sun) abbreviation, which is equivalent to ($1\text{kW}/\text{m}^2$) from solar irradiance energy, and represent the denominator for input power in the efficiency equation:

$$\eta = \frac{P_{out}}{P_{in}} \quad 2.1$$

Therefore, any changing in light intensity leads to change in efficiency too. To change the light intensity lower than 1 sun "Gray Filters", which will attenuate the light intensity will be used, "Gray Filters" function is reducing the photon flux coming from artificial light sources as shown in figure 2.8:

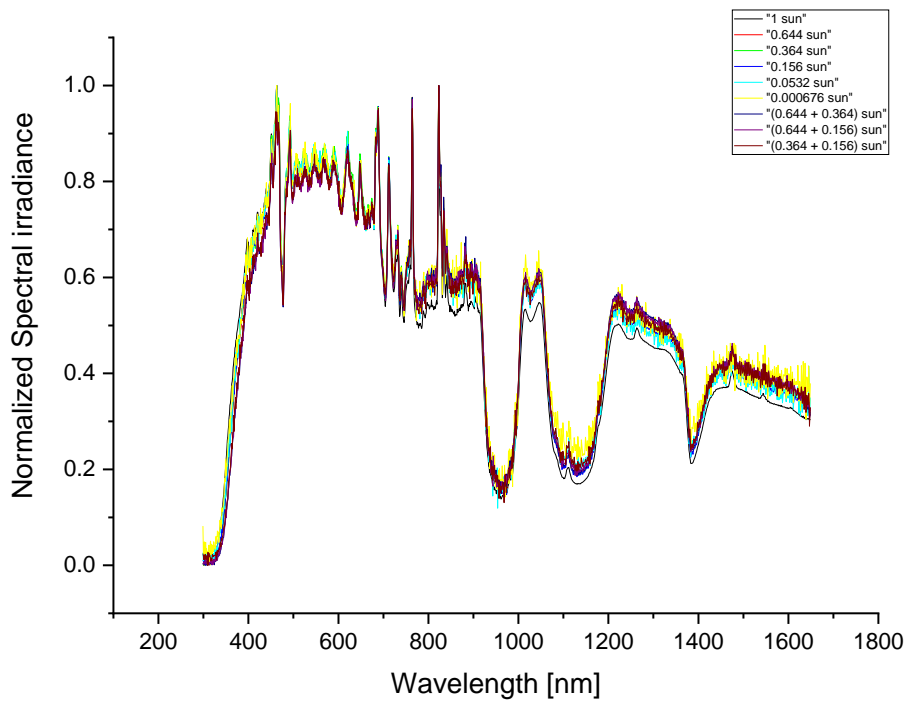


Figure 2. 8: Normalized spectral irradiation for different filters.

Figure 2.8 reveals normalized solar spectral irradiation taken by a sun simulator (AM1.5sumsim). The various gray filters show similar spectra and no deviation from the 1Sun spectra. This is an indication for spectrum uniformly attenuation, due to Gray filters.

Others sources like: LED, fluorescent, and halogen, they are already having low light intensity. Same conditions in order to investigate the solar cell response.

Chapter Three

Experiments

3.1 Optical measurements (UV-VIS spectroscopy measurements)

Improving performance of the solar cell it is a key issue. Therefore, we look for improving the energy harvesting for each cell by minimizing optical losses.

The light beam which comes from the atmosphere has an angle and energy; the incident beams angle plays a key role in beam behavior. Furthermore, the light beam has three components, reflection, absorptance, and transmission. The optical loss in solar cell comes from the reflected part which could not enter the cell, and transmitted part which crosses the cell without being absorbed.

In this study, we will investigate the effect of back contact and layer thickness on the behavior of light in specially design layer the stake in order to determine the parameters which affected on parasitic absorption losses.

It is known that, the layer thickness of single-junction (*a-Si*) or ($\mu\text{c-Si}$) solar cells with (*p-i-n*) configuration affects the light absorption. By increasing the thickness of layer stake lead to increase the possibility of absorbed light in the layer. On another hand, by increasing periodicity of light inside the solar cell layer stake by using reflector back contacts like

hydrogen-doped indium oxide (IOH) or indium zinc oxide (IZO) can improved absorptance.

To determine the parameter responsible for the loss in top layer we will study optical properties of top subcell. To study transmission/reflection measurements we will use LAMBDA 950 UV/Vis Spectrophotometer from PerkinElmer company, with 175-3300 nm wavelength range, and less than 0.05 nm and 0.2 nm resolution for UV/VIS and NIR respectively, and two light sources Tungsten-halogen and Deuterium, as shown in figure 3.1



Figure 3. 1: LAMBDA 950 UV/Vis Spectrophotometer.[10]

Ten samples were prepared at *FZJ, IEK -5*, based on single-junction (*a-Si*) or ($\mu c-Si$) solar cell, with (*p-i-n*) configuration. To study the effect of back contact on the behavior of light in the subcells, four samples were prepared with various ($ZnO/Ag/ZnO$) back contacts and different deposition time for *n-layer* were used in order to get different thickness. Three samples have (*IOH*) back contact and rests of samples without back contact, as will as one sample just glass with *ASAHI-VU* without any layer

stake. The table 3.1 shows the deposition details of the different layer stakes.

Table 3. 1 Deposition parameter for ten single-junction cells based on (*a-Si*) and ($\mu\text{c-Si}$). Current-voltage measurements

Sample	Deposition parameter		
	Back contact	deposition time p-i-i-n(sec)	comment
	ZnO/Ag/ZnO	75,275,3000,90,108	Standard
	ZnO/Ag/ZnO	75,275,3000,108,108	Double a-Si n-layer
18L-183-1	ZnO/Ag/ZnO	75,275,3000,90,220	Double $\mu\text{c-Si}$ n-layer
18L-233-1			
18L-238-1	ZnO/Ag/ZnO	150,275,3000,90,108	Double a-Si p-layer
18L-209-1	In ₂ O ₃ + ZnO	75,275,3000,90,108	Standard
18L-183-4			
18L-233-2	In ₂ O ₃ + ZnO	75,275,3000,180,108	Double a-Si n-layer
18L-238-2	In ₂ O ₃ + ZnO	75,275,3000,90,220	Double $\mu\text{c-Si}$ n-layer
18L-233-3			
18L-238-3	No BC	75,275,3000,180,108	Double a-Si n-layer
18L-309-2			
	No BC	75,275,3000,90,220	Double $\mu\text{c-Si}$ n-layer
	No BC	150,275,3000,90,108	Double a-Si p-layer

3.2 Current-voltage measurements

I-V characteristics curves represents a graphical representation between current and voltage. The I-V characteristic curves are strongly dependent on the temperature and irradiation conditions.

Solar cells are classified as an active electrical device, viz. solar cell generates electrical power by itself, and by using “load switching method” to measure IV-curve for solar cell we will get direct current (DC) as shown

in figure 3.2 According to Ohm's Law ($V=I \times R$) by varying resistance we will generate a various voltage.

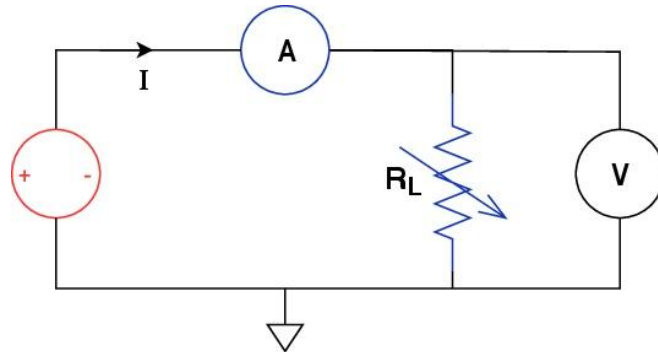


Figure 3. 2: Schematic circuit for load switching.

Figure 3.2 presents a schematic circuit for load swishing method. The solar cell under “*open-circuit condition*”, without any load connected. The current reach to a minimum value, and the voltage across the cell reach to maximum, known as the solar cells *open-circuit voltage* (V_{OC}). By applying another extreme state, “*short-circuit condition*”, through connected positive and negative terminals together. That leads to minimize the voltage to zero, and delivered maximum current flowing out of the cell, known as the solar cells *short-circuit current* (I_{SC}).

The schematic shown in figure 3.3, appear a single diode equivalent circuit for an ideal solar cell, which shows component of the total current produced (I) include current generated by the cell, minus current flows in through the diode (I_D), and through the shunt resistor (I_{SH}).

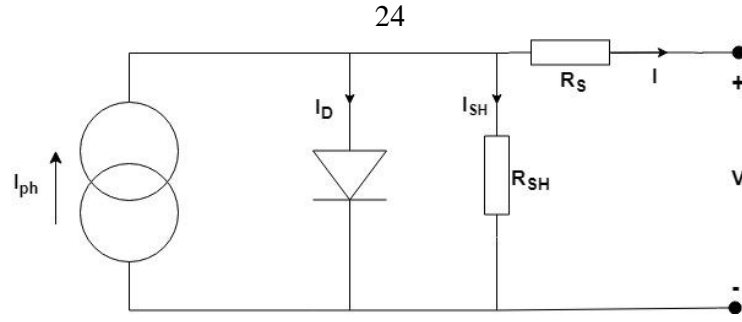


Figure 3. 3: Equivalent circuit for the solar cell.

which can represent it by the following equations:

$$I = I_{ph} - I_0 \left\{ \exp \left[\frac{q(V+IR_S)}{nkT} \right] - 1 \right\} - \frac{I_{RS}}{R_{SH}} \quad (3.1)$$

Where I_0 is reverse saturation current, q elementary charge, n is diode ideality factor, k diode ideality factor, T is absolute temperature.

Figure 3.4, shows IV-characteristic for solar cell. The gray rectangle represents the ideal power from solar cell ($P_{MAX}=I_{SC} \times V_{OC}$), and the pink rectangle represents real and maximum power can gain from solar cell and the ratio between the areas of two rectangles represent fill-factor (FF):

$$FF = \frac{I_{MP} \times V_{MP}}{I_{SC} \times V_{OC}} \quad (3.2)$$

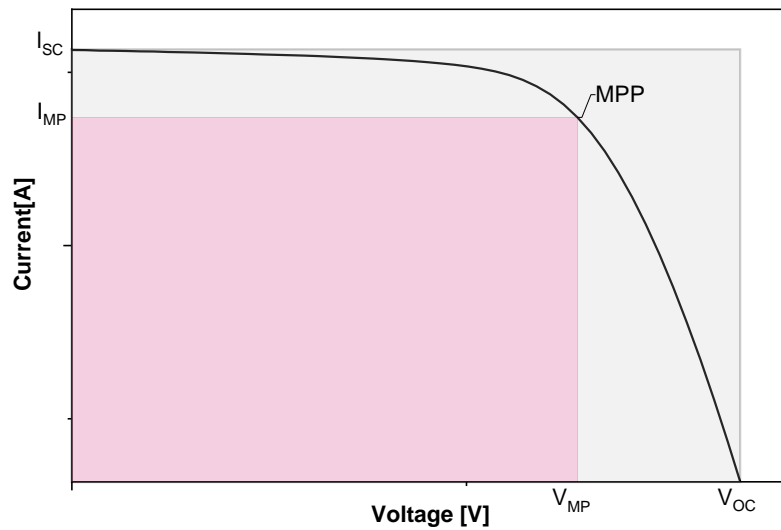


Figure 3. 4: IV-curve of an ideal solar cell

3.3 Differential spectral response (DSR) measurements

The quantum efficiency (QE) of a solar cell is defined as a ratio between the number of electrons collected to incident photon on the solar cell [11]:

$$Q_e(E) = \frac{1}{q} \frac{dJ_{SC}(E)}{d\Phi(E)} \quad (3.3)$$

Where Φ is the photon flux. The QE measurement will be done by GM.QE High resolution quantum efficiency with a grating monochromator. Consisting of a Xenon light source and a Bentham monochromator with a spectral range of 300 - 1100 nm, and 10 nm steps for all SR measurements. 0.7 cm² for 1 cell beam spot with modules up to 10 cm x 10 cm with the setup shown in figure 3.5:



Figure 3. 5: QE monochromator-based setup.

Multi-junction solar cells have a special design where the subcells are connected in series together. This requires a special technique with using a bias light to saturate the not studied subcell, for example, to measure top cell. The bias light has to saturate middle and bottom cell, and wavelength of bias light must be in the effective region of the response of the middle and bottom cell [12].

3.4 Charge/Discharge analysis of 3T solar cell and battery

The second main part of this study was to investigate the ability for charging and discharging of the battery through the PV module which was designed in chapter 2. Achieving a matching between voltage and current from both side -solar cell and battery- is important to avoid overcharging, because that can damage the battery or reverse current from battery to solar cell when lack of light. Therefore, we will depend on IV-curve parameters,

I_{SC} , and V_{OC} to achieve matching for voltage and current between both sides. The 3T-device, module number (17L-312-2) consisting of a a-Si top cell with a p-i-n configuration and n-i-p tandem bottom cell configuration will be exposed to AM1.5 spectrum, (100 mW/cm^2) from sun simulator. Each cell in the module has V_{OC} (0.790 V) and I_{SC} (55.9 mA).

In order to fulfill the requirements for IV characteristics matching between the solar module and the battery for this study a commercially available lithium-ion polymer battery 'ICP501230PS-03' from Renata batteries, with Nominal Voltage (3.7 V), and Nominal Capacity (135 mAh) was used and the picture is shown in figure 3.7:



Figure 3. 6: ICP501230PS-03 Rechargeable Lithium Ion Polymer Battery Pack 3.7 V

Will connect five cells from module in series to obtain voltage around (3.9 V) as shown in figure 3.6b, and connect it with battery directly without converter like shown in scheme in figure 3.8:

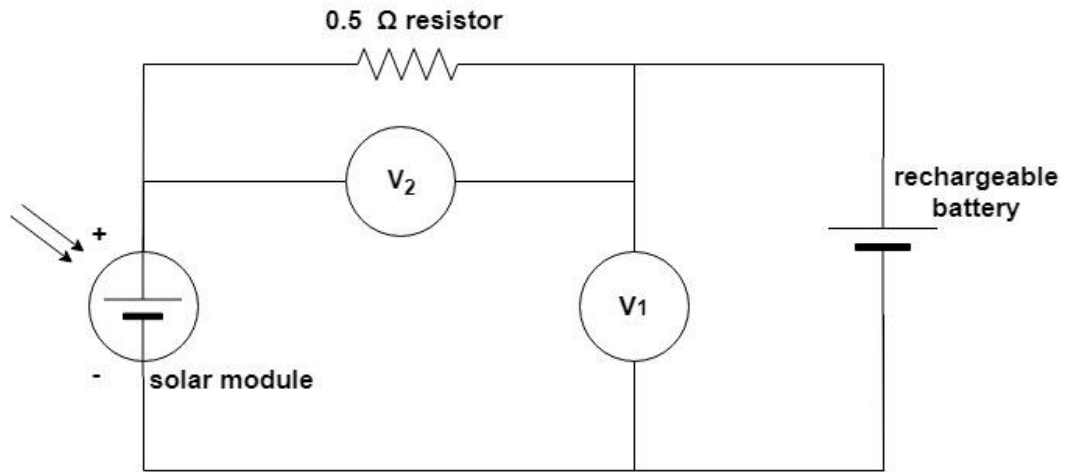


Figure 3. 7: Charge/discharge circuit, current and voltage sense, and battery connected directly with a solar cell. [13]

Chapter Four

Result and discussions

4.1 Development and optimization 3T device

For characterizing 3T-device, sample number (17L-312-3) which was prepared in chapter 2 and shown in figure 4.1a, need to study each sub-cell under illumination. By use thin-film holder and Wacom Solar Simulator WXS-90S-L2 AM1.5GMM which was shown in chapter 2. Will measure three IV-curves for two different connection modes. First one is separate mode for top subcell which composed from (a-Si) with (p-i-n) junction configuration. By applying voltage between (-0.2 to 1 V) and steps (0.02 V) through connection terminal 1 and 2 with positive and negative sense pin on thin-film holder. Second measurement was done by changing position of sense pin from terminal 1 to terminal 3, to measure bottom tandem subcells which are composed from ($\mu\text{c-Si}/\mu\text{c-Si}$) with ($n-i-p/n-i-p$) junction configuration. Another mode of connection it is a parallel mode to measure total current and voltage of the cell under illumination, that need to make interconnection between the top and bottom layer; because the order of cell connection in the real cell as shown in figure 4.1b:

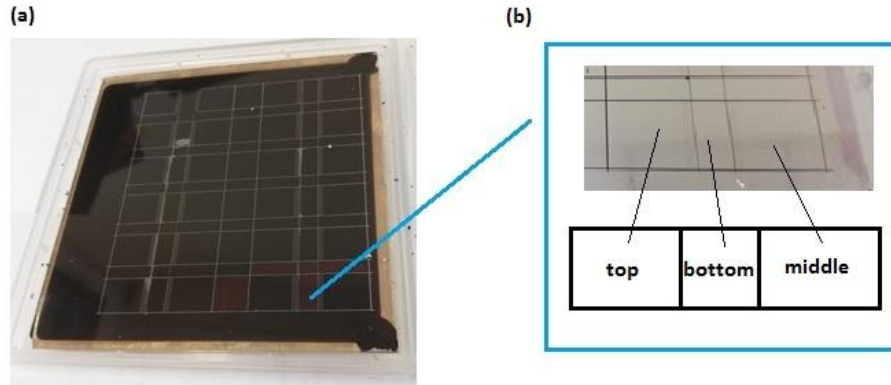


Figure 4. 1: sample number 17L-312-3 (a) top view of the whole sample (b) order of subcell connections.

The positive pin will still be connected with middle subcell, viz. the negative pin will still make the connection with terminal 2 as shown in figure 4.2 which shown a scheme of 3T-device with a diode structure, and positive pin with interconnection which combine between terminal 1 and 3. That possible with the new 3T-device configuration, in contrast to the previous design, which did not allow the measurement of each cell separately.

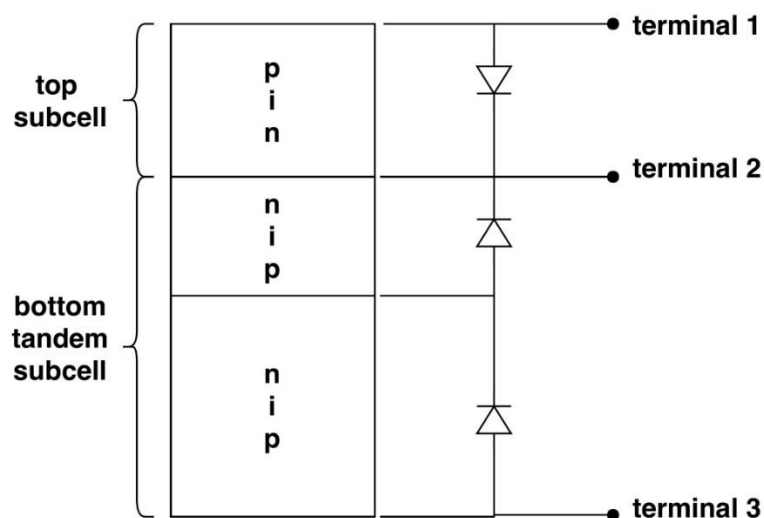


Figure 4. 2: Schematic drawing of 3T-device and diode structure

IV-curve comes by scanning point-for-point of voltage and current, as shown in figure 4.3:

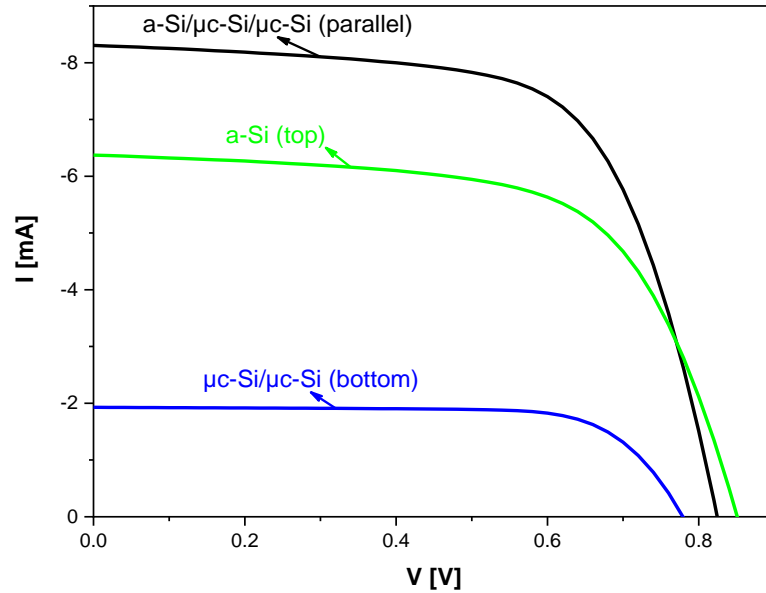


Figure 4. 3: IV-characteristics for a-Si:H top sub cell, $\mu\text{c-Si:H}/\mu\text{c-Si.H}$ bottom tandem sub cell, and the a-Si:H/ $\mu\text{c-Si:H}/\mu\text{c-Si:H}$ cell from sample (17L-312-3)

Three IV curves for 3T-device sample number (17L-312-3) are shown on Figure 4.3. A green and blue IV curve represents separate mode to measure the top and bottom tandem subcells respectively. The black IV curve represents a parallel mode to measure the whole cell. The top subcell (a-Si) has achieved highest open circuit voltage ($V_{OC} = 0.851$ V), and short-circuit current ($I_{SC} = 6.4$ mA), and the bottom tandem subcell has ($V_{OC} = 0.773$ V), and ($I_{SC} = 1.9$ mA), while the parallel mode which represents the total behavior of 3T-device shows an open-circuit voltage that is between the voltage of top and bottom tandem subcell ($V_{OC} = 0.823$ V). This is due to "mismatch-voltage" between top and bottom tandem subcell. While the fill factor limited by top subcell, the total efficiency was increased due to

multi-junction solar cell technology. For ideal case when two voltage sources are connected in parallel, the voltage of two sources must be equal, otherwise the lower one will limit the total voltage to the average value. Although the new device design with three terminals overcome on "*mismatch-current*" with the additional third terminal but it can create *mismatch in voltage* in the total cell. On the other hand, the current of the 3T-device is ($I_{SC} = 8.3 \text{ mA}$), as presented in table 4.1:

Table 4. 1 PV parameter of 3T-device, sample (17L-312-3), cell 10, under AM1.5 illumination

Connection mode	PV parameters			
	$V_{oc}[V]$	$I_{sc}[mA]$	FF[1]	$\eta[1]$
Separate – top	0.851	6.4	64.6	7.0
Separate – bottom tandem	0.773	1.9	74.0	2.2
Parallel – total cell	0.823	8.3	65.5	9.0

To achieve optimum performance for 3T-device, we should achieve maximum matching of the voltages of the top and bottom tandem. By improving the voltage of the bottom subcell we can achieve to improvement of the efficacy of the whole device.

Figure 4.4 presents the quantum efficiency of 3T-device, sample number (17L-312-3). The *a-Si:H* top subcell achieve QE of about (80%) as expected. The current density of the *a-Si:H* top cell is (12.5 mA/cm^2) that is a little bit lower than current density measure by IV measurements. The tandem sub cell based on $\mu c\text{-Si:H}/\mu c\text{-Si:H}$ are limited by middle $\mu c\text{-Si:H}$ cell. The current density collected from middle and bottom cell is ($3.377, 5.076 \text{ mA/cm}^2$) respectively. In this case we cannot avoid current

mismatching in the tandem cell therefore the current density of the total cell is 3.9 mA/cm^2 .

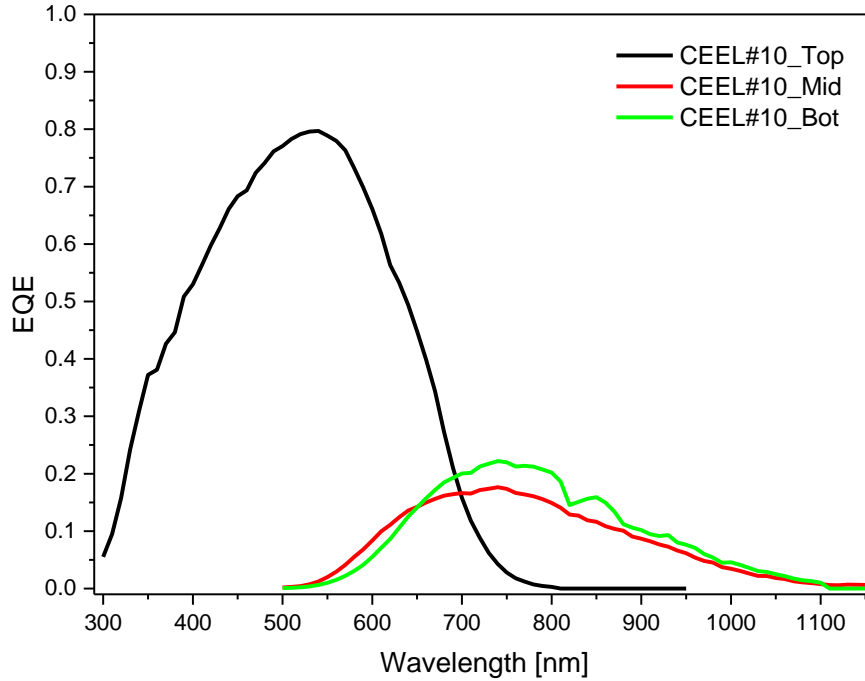


Figure 4. 4: External Quantum Efficiency of sample number (17L-312-3)

To solve the mismatch-voltage in the cell we have to improve the voltage of bottom tandem subcell, by increasing the deposition time. Will fabricate two sample with two different times of deposition for intrinsic layer (*i-layer*) of the middle subcell. First sample number (18L-203-2), with (60 min) deposition time for (*i-layer*), and second cell number (18L-197-2) with (70 min) deposition time for (*i-layer*). All other parameters it is the same parameters of first sample number (17L-312-3).

Figure 4.5 shows the I-V characteristics for two samples. On the left side, the sample number (18L-203-2, and sample number (18L-197-2) in

right side. The top and bottom tandem subcells are measured separately and their I-V characteristics curves are shown in green and blue colours respectively. A parallel mode was used to measure the whole cell (see the black) IV curve. The sample number (18L-197-2) shows almost matched voltages between the *a-Si:H* top and the bottom tandem sub cells. The PV parameters for the 2 samples are presented in table 4.2.

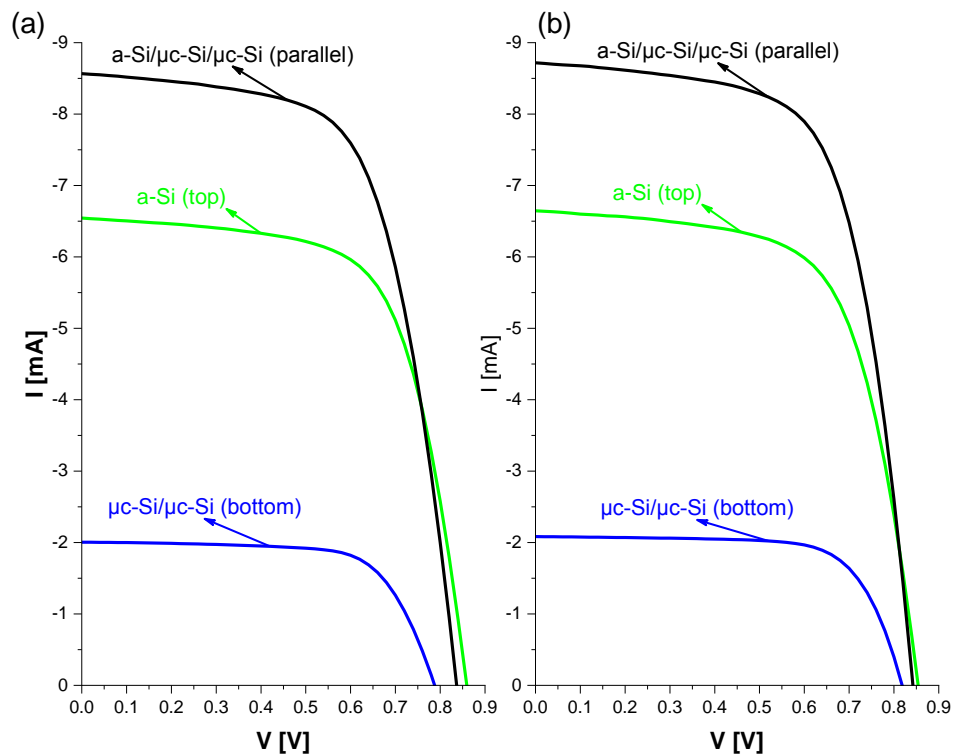


Figure 4. 5 IV-characteristic curve (a) sample number (18L-203-2) (b) sample number (18L-197-2).

Table 4. 2 PV parameter of 3T-device, samples (18L-203-2, 18L-197-2), cell 10, 09 respectively under AM1.5 illumination

Connection mode	PV parameters			
Sample# 18L-203-2	$V_{oc}[V]$	$I_{sc}[mA]$	FF[1]	$\eta[1]$
Separate – top	0.858	6.5	65.7	7.6
Separate – bottom tandem	0.773	2.0	69.5	2.2
Parallel – total cell	0.836	8.6	63.9	9.2
Sample# 18L-197-2	$V_{oc}[V]$	$I_{sc}[mA]$	FF[1]	$\eta[1]$
Separate – top	0.853	6.6	64.8	7.3
Separate – bottom tandem	0.816	2.1	71.2	2.4
Parallel – total cell	0.841	8.7	65.7	9.6

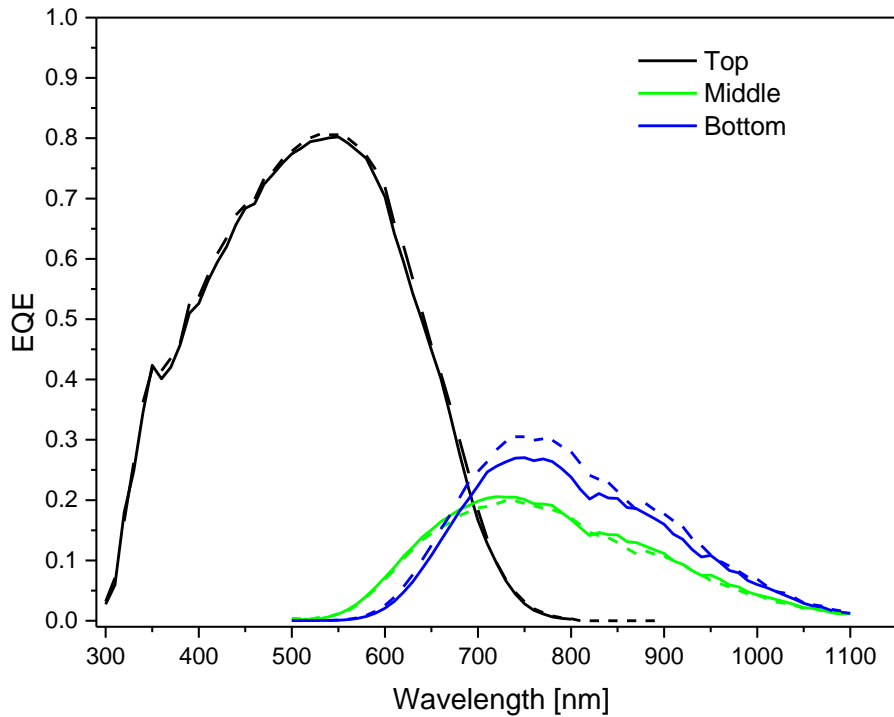


Figure 4. 6: External Quantum Efficiency of 3T-device, the continuous line represent sample number (18L-197-2) cell number (09), and the dashed line represent sample number (18-203-2) cell number (10).

Figure 4. 6 shows quantum efficiency of 3T-device with a different of the middle layer of the tandem sub cell. QE spectra of the top and middle subcell from the two samples shows the same response under AM1.5 illumination. Increasing thickness of middle subcell results in decrease of the current density ($5.1, 4.9, 4.5 \text{ mA/cm}^2$) of the bottom subcell for samples number (17L-312-2, 18L-203-2, 18L-197-2) respectively, while the current density of the middle subcell increases ($3.4, 3.6, 3.8 \text{ mA/cm}^2$) for samples number (17L-312-2, 18L-203-2, 18L-197-2), respectively.

4.2 The electrical loss in parallel mode

3T-device consists two main subcells, namely top and bottom tandem. The power generated is not ideal, so can be classified the electrical losses into two parts in 3T-device. First one is electrical losses due to the current limitation which is occurs in the bottom tandem subcell. The second part of the electrical losses, which due to the drop voltage. Figure 4.7 shows scheme and voltage and current density for each subcell.

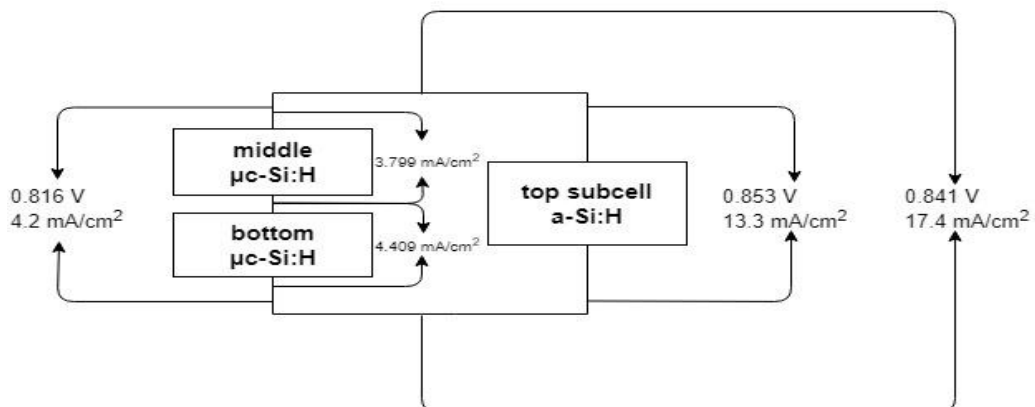


Figure 4. 7: scheme for configuration of 3T-device and PV-parameters for each subcell for sample number (18L-197-2) cell number (09).

Table 4.3 shows the losses due to mismatching. The matching reached 95.67% and 86.16% in the voltage and current respectively.

Table 4. 3 Electrical losses in parallel mode

Losses type	mismatch-voltage	mismatch-current
Subcell	top and bottom tandem	middle and bottom
Loss [mW/cm^2]	0.208	0.170
Matching [1]	95.67	86.16

4.3 Optical loss analysis

To find parameters which affect parasitic absorption in 3T-device, we focus on the layers marked in figure 4.8. We have deposited a single-junction *a-Si:H* solar cell with various back contact configurations and Asahi-UV transparent conductive oxide as a front contact.

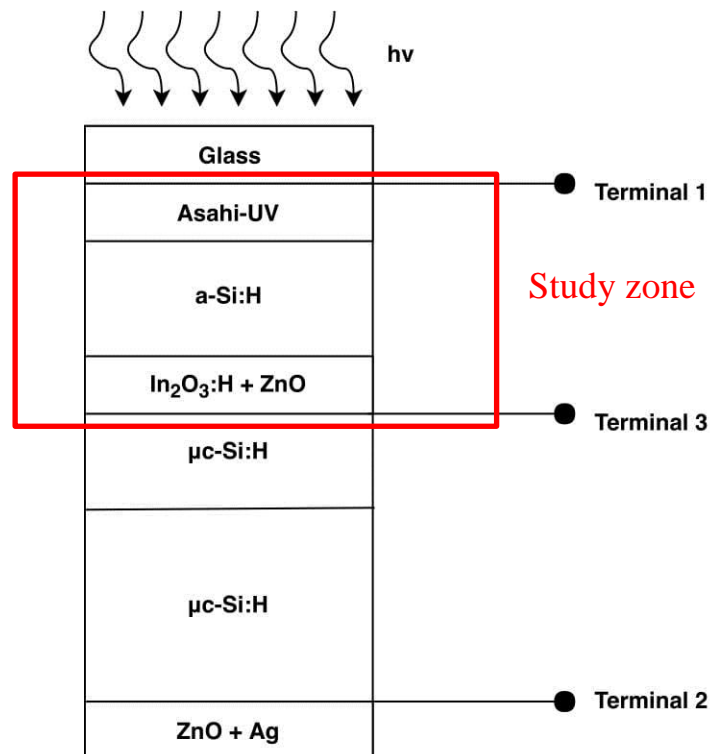


Figure 4. 8: Schematic drawing of 3T-device

Figure 4.9 shows the absorption spectra of the amorphous thin-film solar cells with different thickness for n - and p - layers, and different back contact. Additionally, absorption spectra of *Asahi-UV* together with the EQE spectra of the top and middle a - $Si:H$ and μc - $Si:H$ solar cells are presented. Changing the back contact has a clear effect on the behavior of absorption, cells without back contact and cells with *IOH* back contact has a lower absorption as compared to back contacts with *ZnO*. *ZnO* layer works as back reflector of the light in direction to the a - $Si:H$ layers. The remaining amount of optical losses due to absorption of light in *Asahi-UV*, as shown in figure 4.9.

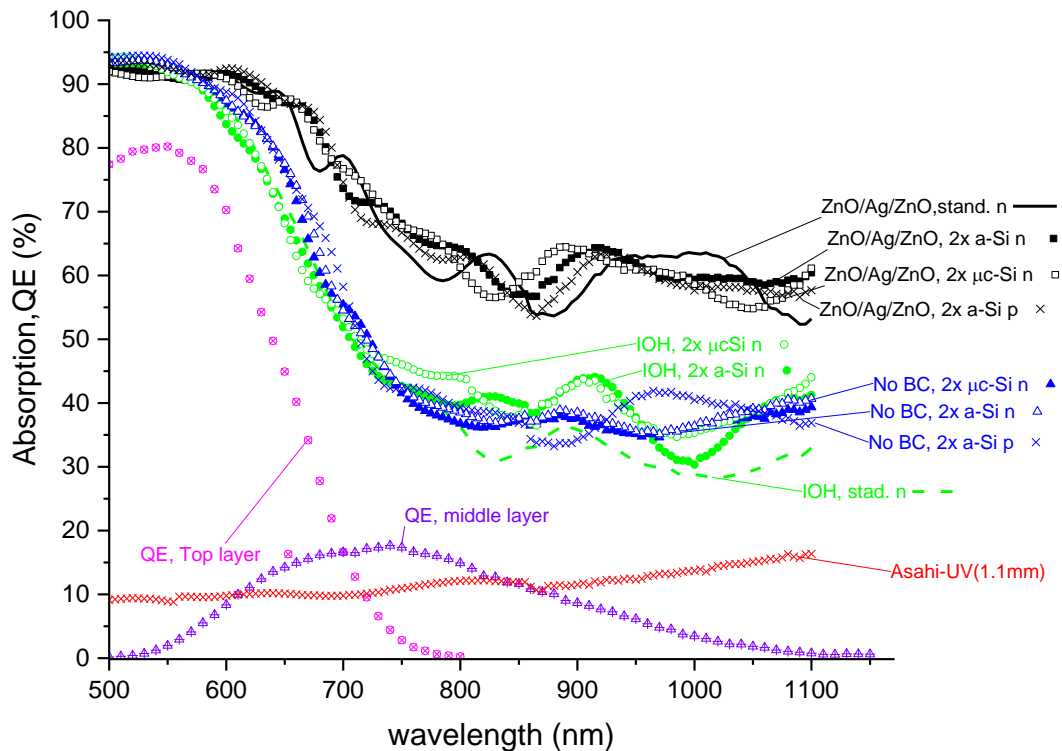


Figure 4. 9: Absrption spectrafor a-Si:H single junction cells with different back contact and different thickness of the n-layers.

4.4 Dependence of PV parameters on Illumination intensity and spectra for 3 T triple-junction solar cells

Studying behavior 3T-device under low light intensity sources such as LED, halogen and tube can give us insight for the performance of the 3T-device based on triple junction cell under low illumination intensity when integrated to a battery. As mentioned in chapter 2 in figure 2.8, was used gray filters to uniformly attenuated for the spectrum of light sources. Figure 4.10 shows the open –circuit voltage and FF of each subcell of the 3T-device in separate mode and total cell in parallel mode. The V_{OC} (figure 4.10 (a)-(d)) of the a-Si:H top cell shows lower decrease of the voltage with decreasing the light intensity for all light sources as compared to the bottom cell. Unfortunately, the V_{oc} of the whole 3T-device measured in parallel mode follow the V_{oc} values of the bottom cell. On the other hand, the fill factor of the a-Si:H top cell slightly increase followed by almost constant behavior with decreasing the J_{SC} for illumination under AM1.5 and LED. and spectral response for each light source. The top subcell shown the highest V_{OC} and FF under different light sources, while bottom tandem subcell limited by top subcell, therefore the total behavior of the cell which represented in black square limited by bottom tandem subcell.

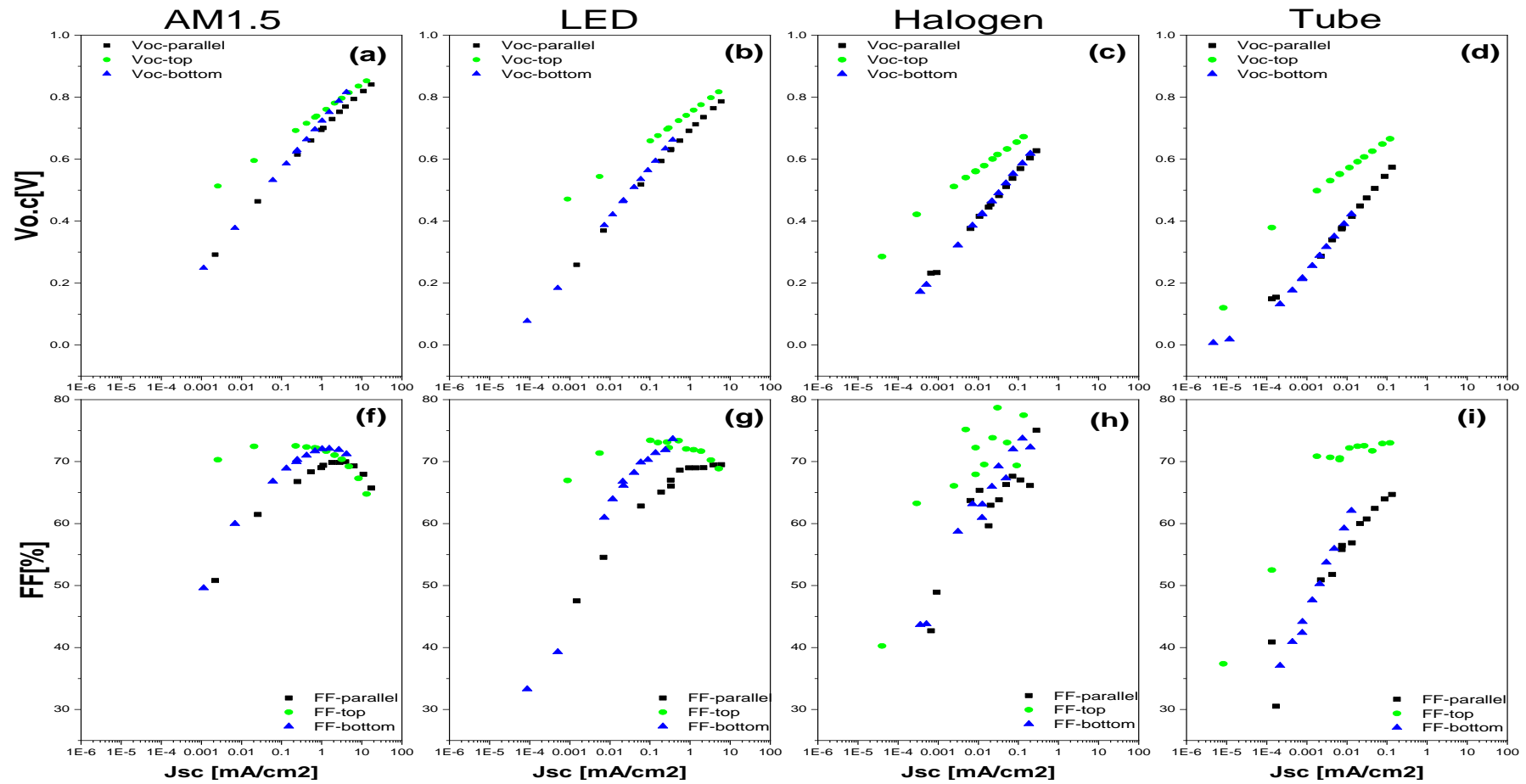


Figure 4. 10: Open-circuit voltage ((a)-(d)) and fill factor ((f)-(i)) for 3T-device measured in parallel mode(black square, total cell) and separate mode (green circle and blue triangle represent top and bottom tandem subcell, respectively)

To evaluate the total performance of the 3T-device we will calculate the efficiency, i.e. the ratio between the electrical power outputs to the input power from the light source.

$$\eta = \frac{J_{SC} \times V_{OC} \times FF}{P_{in}} \quad (4.1)$$

Where J_{SC} , V_{OC} , FF , and P_{in} are the short-circuit current density, open-circuit voltage, fill factor, and the input illumination power, respectively. As shown in Figure 4.11, the power input changed with the illumination power, therefore we have to determine the power input while changing the illumination power via filters, and calculate the power input for each intensity. The linear relationship between the J_{SC} and illumination irradiance [14] is a requirement for this.

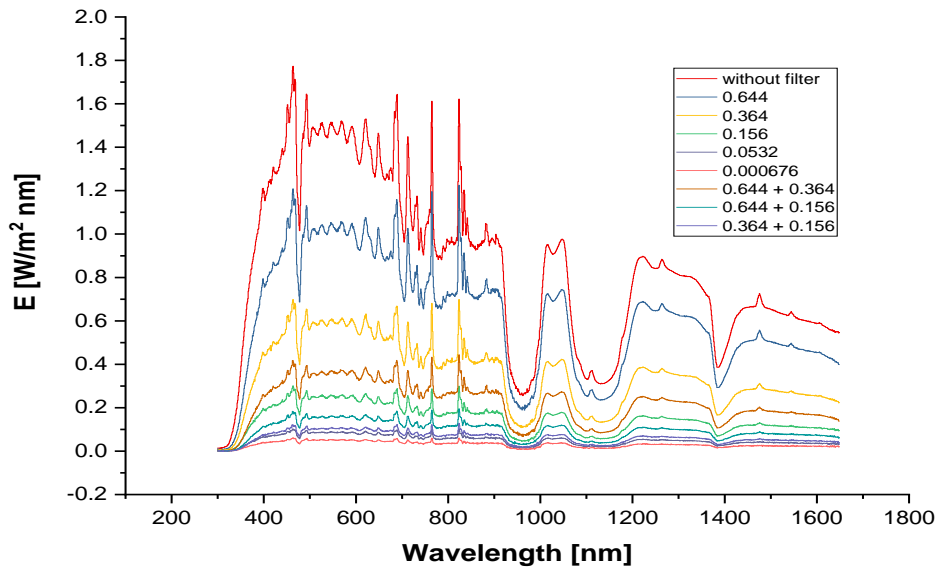


Figure 4. 11: Spectral irradiation for different filters.

Figure 4.12 shows the calculated efficiency for 3T-device based on triple junction solar cells (a-Si:H/ μ c-Si:H/ μ c-Si:H) measured in separate mode in in parallel as compared to single junction a-Si:H, μ c-Si:H and as

well as the 2T device based on triple junction solar cell (a-Si:H/ $\mu\text{c-Si:H}/\mu\text{c-Si:H}$) as a function of J_{SC} for different light sources. The highest efficiency is recorded for 3T device based on triple junction solar cell (a-Si:H/ $\mu\text{c-Si:H}/\mu\text{c-Si:H}$), measured in parallel mode under LED light source (16.4%) (see Figure 4.11(a). Furthermore, by comparing the top and bottom tandem subcell (Figure 4.11(b)) with single-junction cells (Figure 4.11(c)), we have observed that their efficiency is lower as compared to the single a-Si:H and $\mu\text{c-Si:H}$ solar cells. Very likely Table (table 4.4, table 4.5) tabulates the values of the efficiency and current density (J_{SC}) of 3T-device in both modes (parallel and separate) under different light sources (AM1.5, LED, tube, and halogen) and single-junction efficiencies [14]:

Table 4. 4 Efficiencies for 3T-device and 2T triple junction solar cells and single-junction a-Si:H and $\mu\text{c-Si:H}$ solar cells.

Mode\light source		AM1.5	LED	Tube	Halogen
Separate	Top	6.39%	14.60%	11.62%	2.34%
	Bottom	2.10%	0.90%	0.61%	2.95%
Parallel	Total	8.38%	16.42%	9.55%	4.43%
Single-junction	a-Si:H	10.19%	19.74%	14.78%	1.59%
	$\mu\text{c-Si:H}$	8.57%	11.25%	6.55%	2.34%
	Type A	11.01%	9.01%	6.22%	0.99%

Table 4. 5 Current density (J_{SC}) for 3T-device and 2T triple-junction solar cells and single-junction a-Si:H and $\mu\text{c-Si:H}$ solar cells in (mA/cm^2) unit.

Mode\light source		AM1.5	LED	Tube	Halogen
Separate	Top	13.3	5.2	0.12	0.13
	Bottom	4.2	0.37	0.013	0.20
3T Parallel	Total	17.4	6.0	0.13	0.28
Single-junction	a-Si:H	16.0	3.0	0.10	0.16
	$\mu\text{c-Si:H}$	24.4	3.4	0.15	0.40
2T Triple-junction cell	Type A	8.1	0.40	0.02	0.04

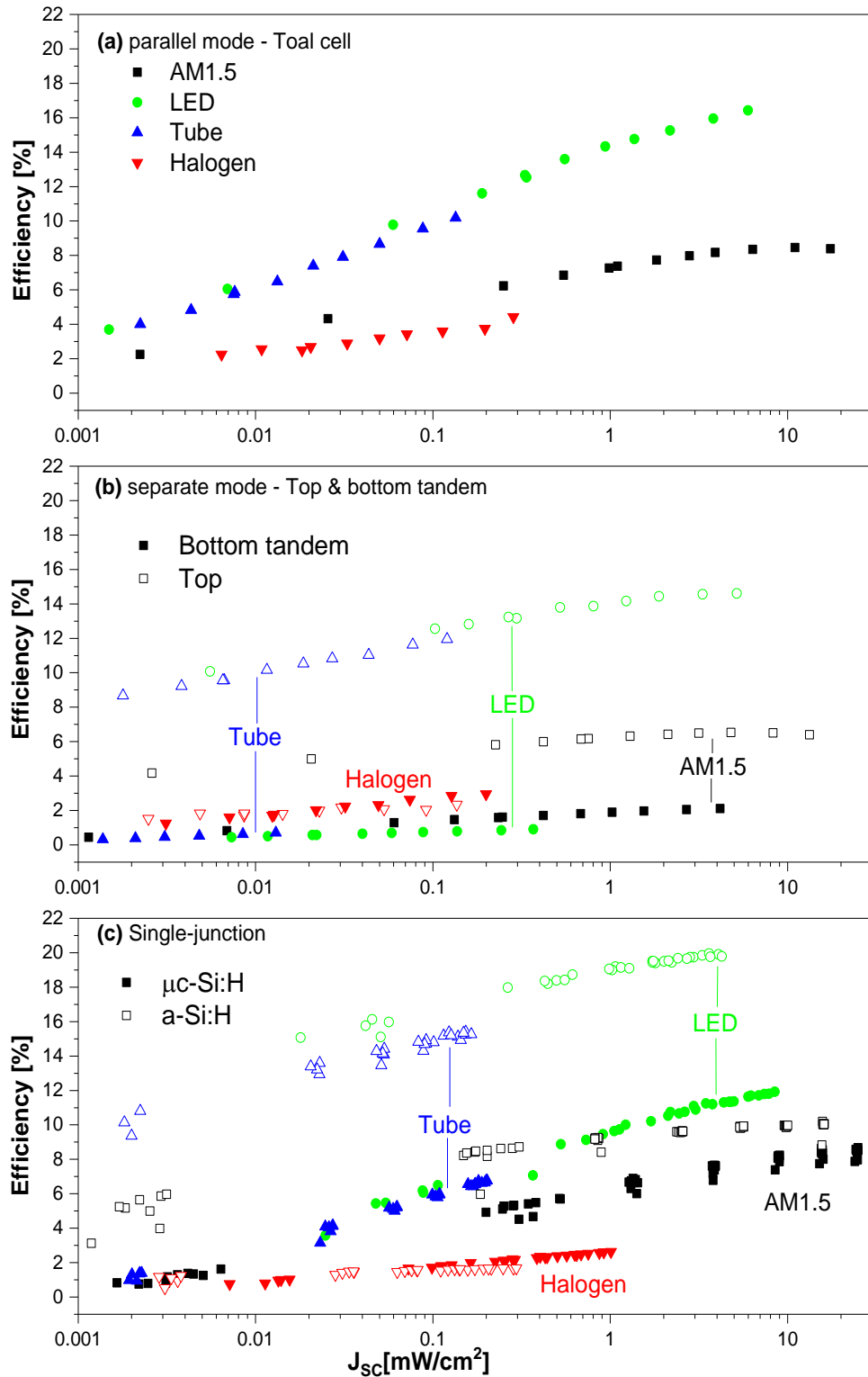


Figure 4. 12: Efficiencies of (a) 3T device based on triple junction solar cell in parallel mode (b) a-Si:H top and $\mu\text{c-Si:H}/\mu\text{c-Si:H}$ tandem- subcells in separate mode (c) single-junction a-Si:H and $\mu\text{c-Si:H}$ solar cells [14] under different light sources.

4.5 Comparison between 2T and 3T triple-junction solar cells

To evaluate behavior of 3T-device before testing for charge/discharge cycle experiments with a battery. A comparison between the PV parameters of previous design 2T-device [13] and the new design 3T-device based on the layer stark triple junction solar cell (see figure 4.12). It is observed that the efficiency of 3T-device is similar to efficiency of 2T-device under tube and halogen light source, but 3T-device has higher efficiency under LED light source.

The Voc and FF for 2- and 3-terminal triple junction a-Si:H/ μ c-Si:H/ μ c-Si:H solar cell are decreasing at with decreasing the Jsc, i.e. illumination intensity as expected. However, the Voc and FF values for 3-terminal devices are lower (see Figure 4.12 (b) and (c) as compared to 2-terminal device. Finally, the efficiency for 2- terminal device is a way higher for LED and AM1.5 sources and reaches about 16.4% and 11.7%, respectively at the highest illumination intensity as compared to 2-terminal devices due to higher Jsc values measured for these devices.

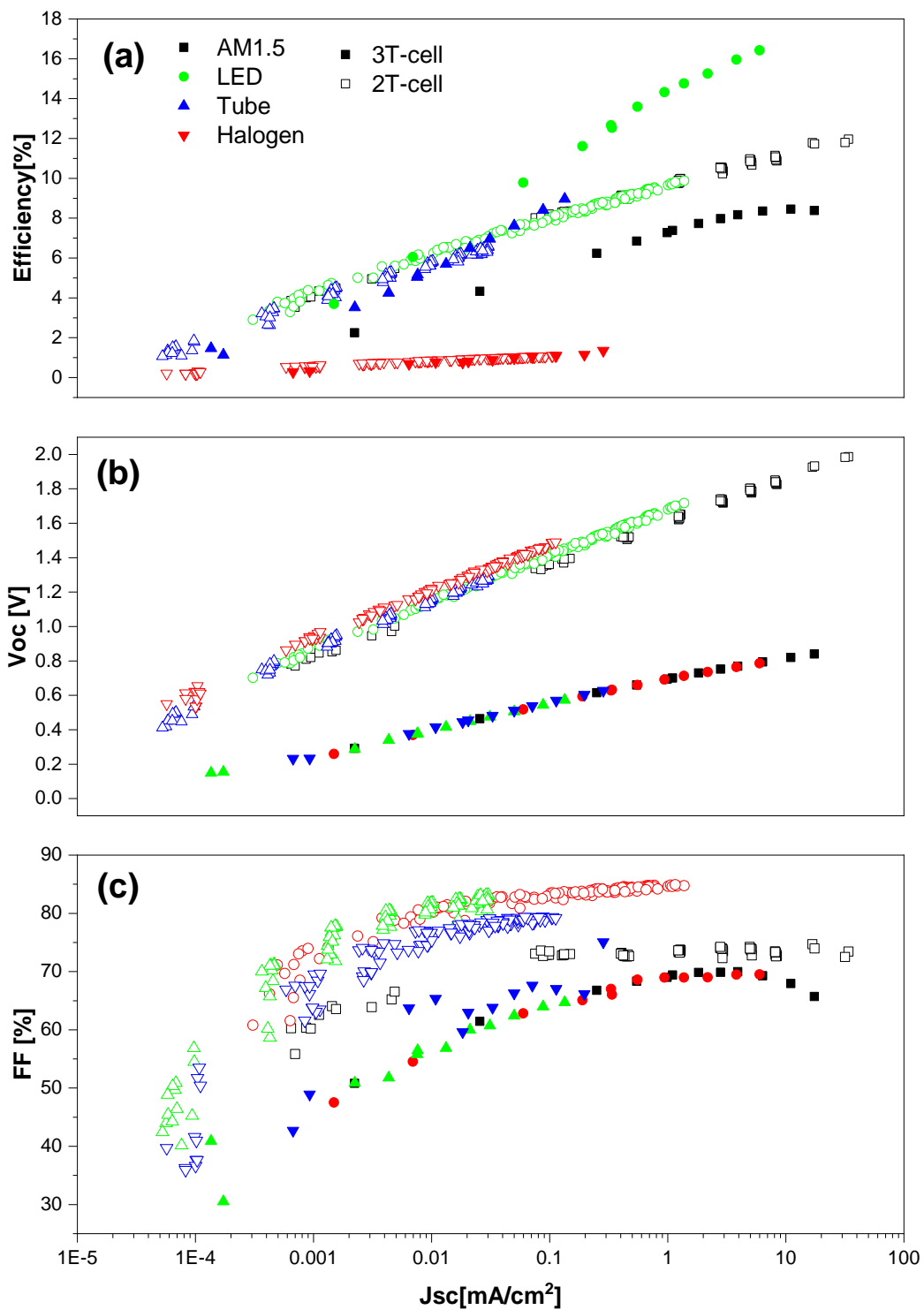


Figure 4. 13: Comparison between 3T- and 2T-device based on triple junction a-Si:H/ μ c-Si:H under different light sources (a) efficiency (b) open-circuit voltage (c) fill factor.

4.6 Comparison between 3T, SHJ, and Perovskite solar cell

In the last part from chapter 4, we will show a comparison between three different types of solar cell as a function of various light intensity for different light sources.

Figure 4.14 ((a)-(b)) shows the *efficiency*, V_{OC} , and FF , for three type of solar cells, perovskite, silicon heterojunction (*SHJ*), and 3T-device. The perovskite solar cell was prepared at IEK-5 lab by using the solution method has the best performance under different light sources and the structure of perovskite solar cell is shown in figure 4.13 (a). The schematic drawing of silicon heterojunction solar cell (*SHJ*) is shown in figure 4.13 (b).

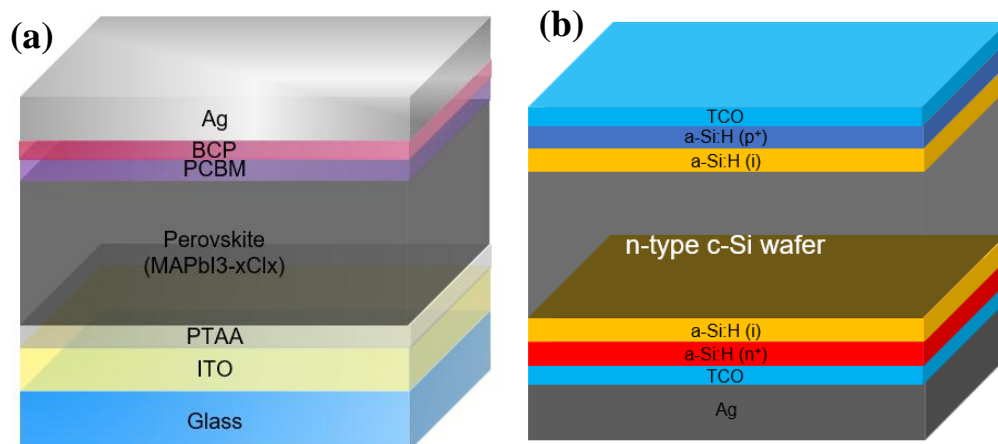


Figure 4. 14: Schematic drawing of (a) Perovskite (b) SHJ solar cells.

Figure 4.15 show efficiency, V_{OC} , and FF for perovskite, SHJ, and 3T-device under different light sources and light intensities. Perovskite has the highest efficiency under an indoor light source (LED) and reaches about 29%. Moreover, Perovskite has the highest V_{OC} reaches about 1.24 V. the

second highest efficiency under indoor light source recorded for 3T-device, reach 16.4%. On the other hand, and under AM1.5 SHJ recorded the highest efficiency reach about 15.4%. On the contrary, lower FF under low light intensity.

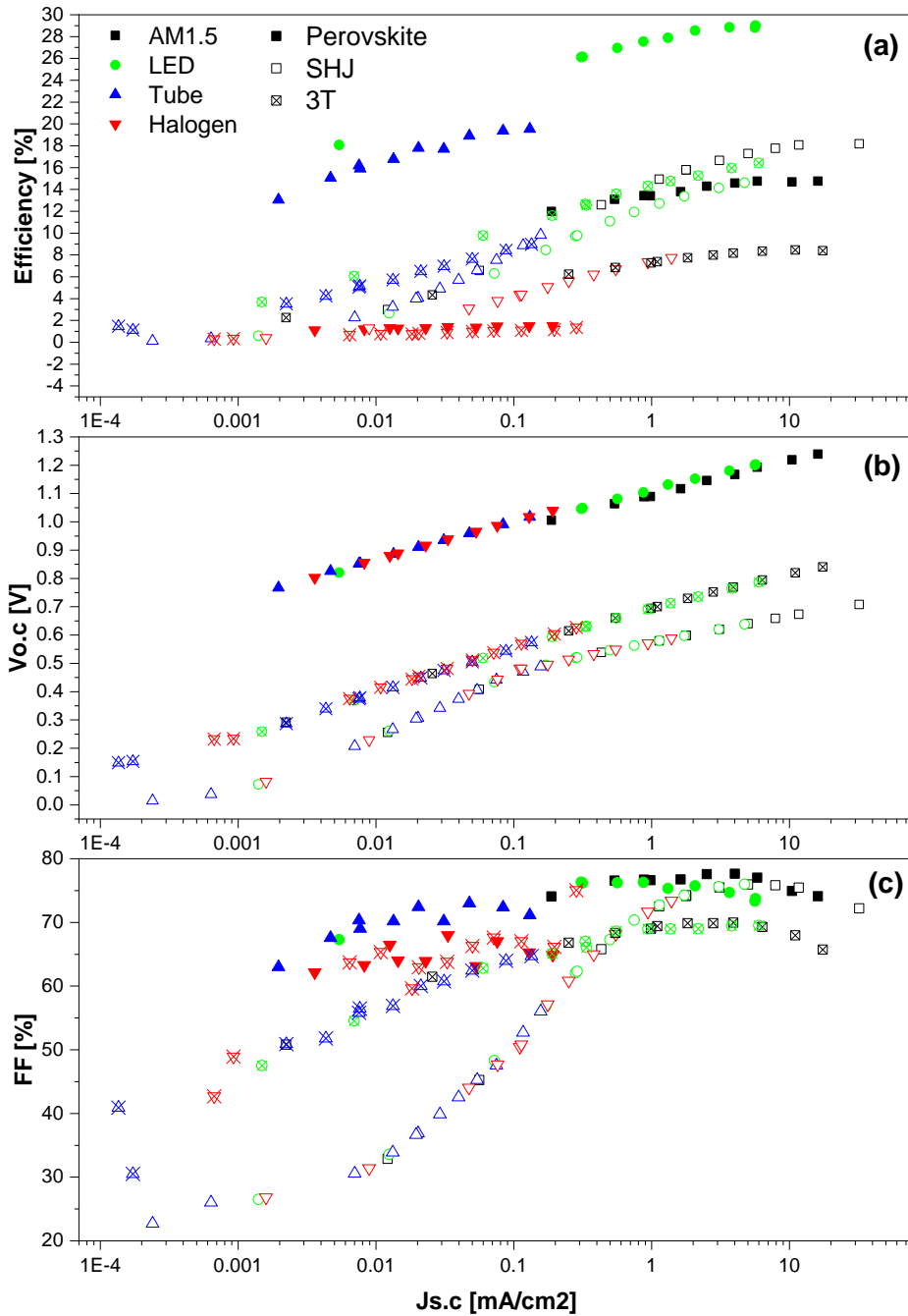


Figure 4. 15: Comparison of PV parameters(a) efficiency (b) open-circuit voltage (c) fill factor for 3T-device, Perovskite, and SHJ as a function of $J_{s.c}$ for different light sources.

That difference between the three types of solar cells is due to different spectral response for each type under each light source. Figure 4.16 and 4.17 shows the EQE of perovskite, SHJ, and 3T-device with a spectrum of AM1.5 (sun simulator), LED, Tube (fluorescent), and halogen lamps. The wavelength range covered by SHJ for AM1.5 light source is wider than the range covered by perovskite and 3T-device, that leads to better performance for SHJ under AM1.5 at long wavelengths (1150 nm). At low wavelength the EQE spectra of Perovskite solar cells and LED spectra match very well. As result we have observed that the PV parameters of perovskite solar cells reach the highest values as compared to SHJ and 3T device.

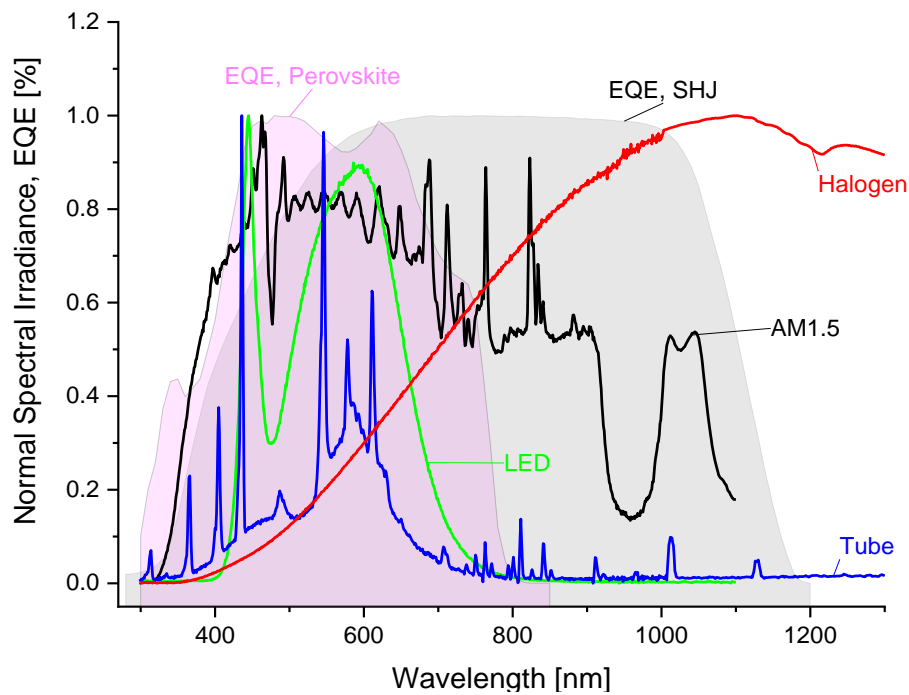


Figure 4. 16: Normalized spectral irradiance of the different light sources used for this study in comparison with the normalized external quantum efficiency (EQE) of perovskite and SHJ solar cells.

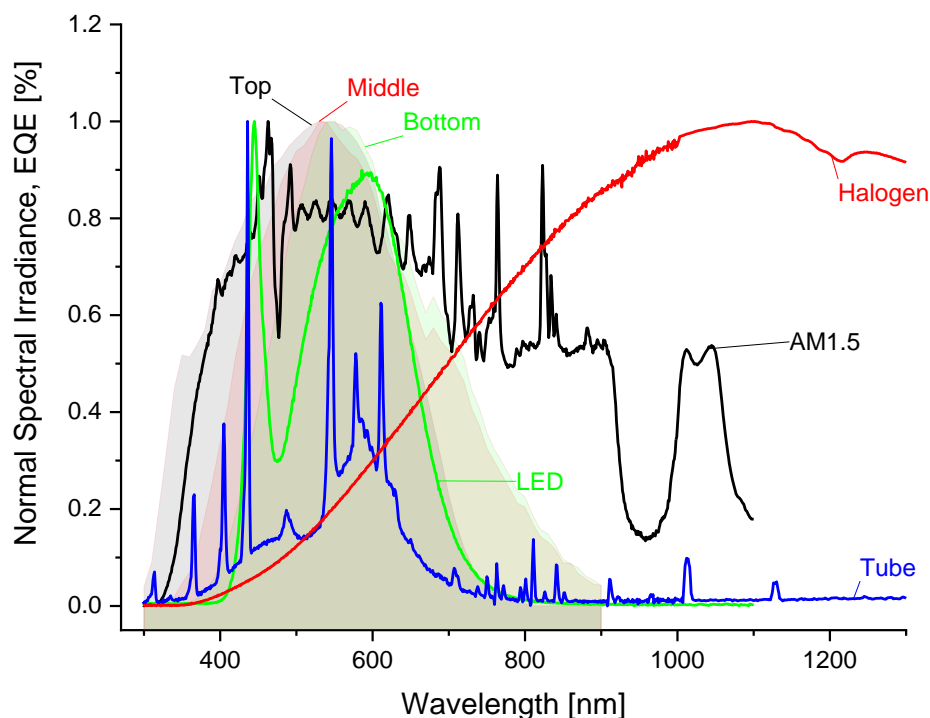


Figure 4. 17: Normalized spectral irradiance of the different light sources used for this study in comparison with the normalized external quantum efficiency (EQE) of 3T-device subcells.

4.7 The performance of integrated three-terminal/triple-junction thin-film module and a lithium Ion battery

After studying the behavior of 3T-triple junction a-Si:H/ μ c-Si:H/ μ c-Si:H solar cells. In the following, we prepare a 3T- module consisting of five cells connected in series for providing the appropriate voltage of 3.9 V as tabulates in table 4.6, and figure 4.18 shows the IV characteristic for one cell and five cells, as already introduced in section 3.4. To charge the battery Figure 4.17 reveals that the voltage of the battery is around 3.4 V at the beginning of charging. According to the datasheet of Renata battery, the cut-off discharge voltage is (3 V), and nominal voltage is (3.7 V). So, the voltage driving from cell it is around (3.9 V, 5.4% excess voltage) it is

enough for doing smooth charged cycle. The full charge cycle takes (2.4 h) note that time needed to reach to nominal voltage it is around (0.26 h) but after this time the current is still flowing into the battery, the voltage increases until reach to stability, then beginning in discharge phase without load.

Table 4. 6 IV Parameters of the module.

	η [%]	FF [%]	I_{SC} [mA]	V_{OC} [V]
1 cell	7.1	64.6	55.9	0.790
5 cells	7.1	64.1	55.9	3.978

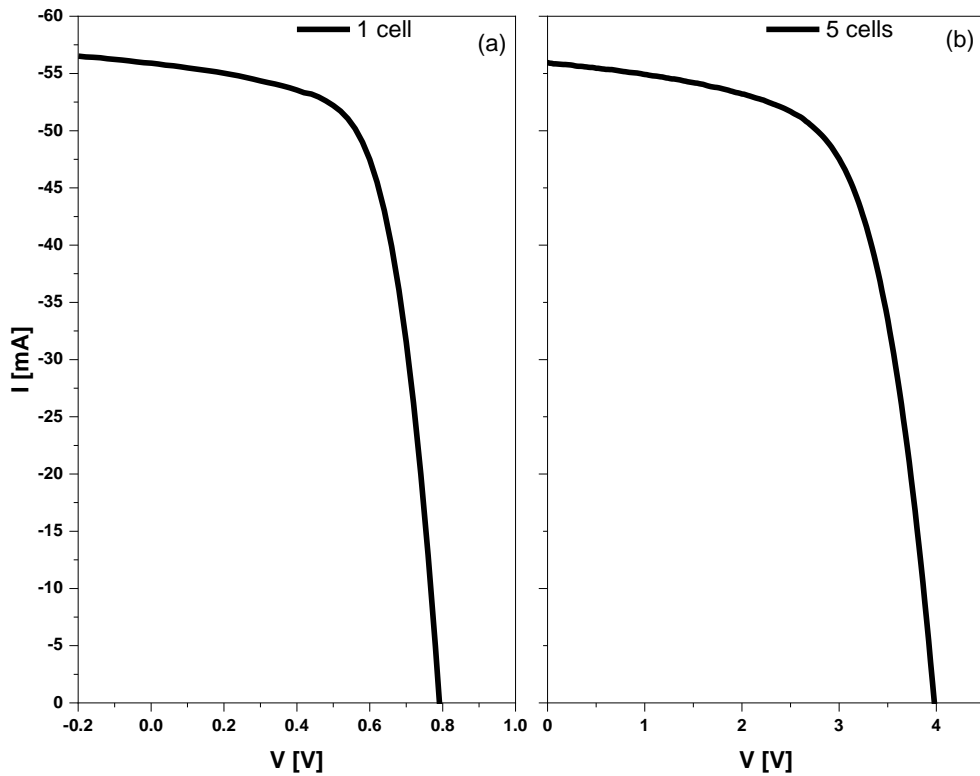


Figure 4. 18: Characteristic of 3T-device under AM1.5 illumination (a)IV curve for one cell from the module (b) IV curve for five cells connected in series.

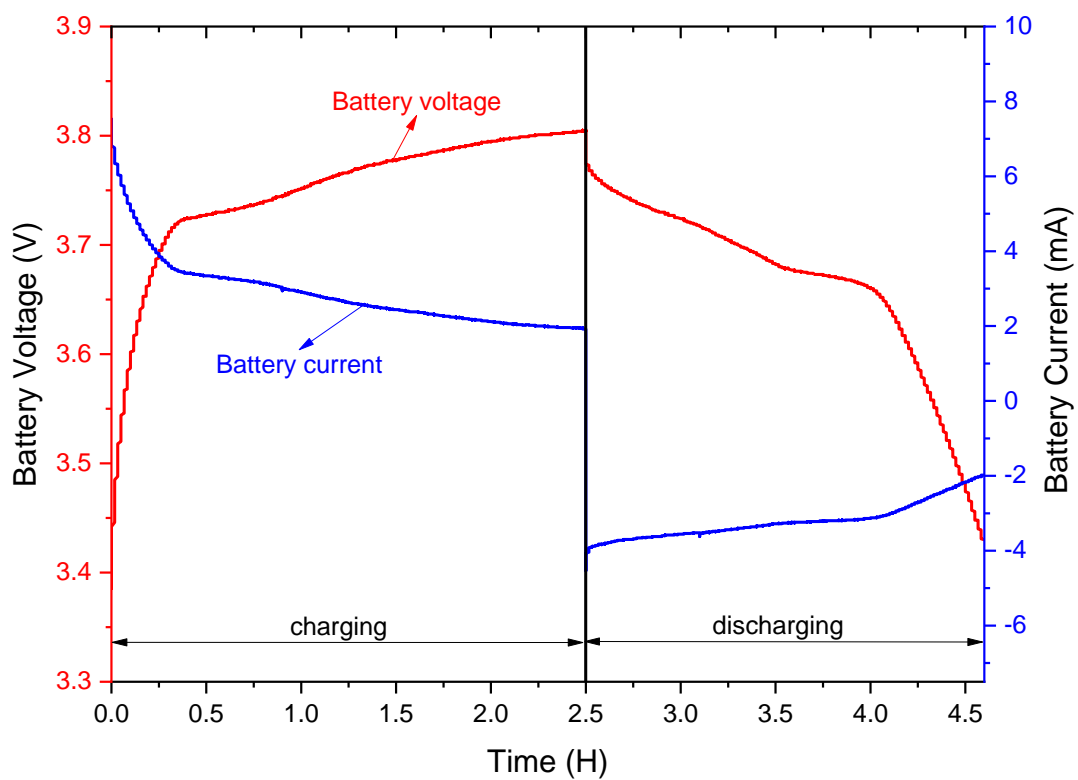


Figure 4. 19: Charge/Discharge profile for 3T-device with (3.7V, 135mAh) battery.

Chapter five

Conclusion and Future Work

Development of suitable PV module for PV-battery device is the first aim of this study. We focus on thin-film silicon technology due to the possibility to achieve a broad band of voltages. We developed a triple-junction solar cell based on a-Si:H/ μ c-Si:H/ μ c-Si:H in 3T-configuration and by optimize the thickness of middle sub cell we obtain the best performance of ... for sample number (18L-197-2) with (70 min) deposition time for *i-layer*.

We have investigated 3T-device under different light sources such as AM1.5sumsim and indoor light sources (LED, tube, and Halogen). The illumination intensity was also varied from 1 sun to different values by using 'gray filters' to attenuate light intensity.

Optical losses analysis was performed by changing the thickness of n-doped layers and using different types of 'back contact' (*IOH*, *ZnO*). Transmission/reflection measurements for each type of back contact combination reveals that of the n-layer thickness has not a strong influence but using *ZAZ* as a back-contact results in a higher absorption as compared to the other back contact (*IOH*, No back contact) used in this work.

On the other side, the comparison between 3T- and 2T-device shows good efficiency 3T-device under indoor light source compared to 2T-device especially under LED light source due to overlap a spectral response of LED and 3T-device.

In the last stage of our study, connected 3T-device with commercial battery was used to investigate the ability of 3T-device to charge and discharge a battery.

Future work of PV-battery can be by investigating the contact/interface between PV and battery integration. Also, do an actual monolithic integration of PV and battery without control electronics. Testing of integrated PV-battery with control electronics in the three-terminal configuration.

References

- [1] Embargo OOJUDoS, **Office of the Historian**. Embargo 1973–1974.
- [2] **Department of Economic and Social Affairs**. 2018 Energy Statistics Pocketbook. 2018, Jun.
- [3] United Nations Statistics Division. 2018 **energy statistics pocketbook**. Energy Statistics Newsletter 2018, Jun 28 2018, Jun.
- [4] UNEP; Bloomberg New Energy Finance; **FS-UNEP Collaborating Centre**. Share of renewable power in energy generation globally from 2007 to 2017 2018, July 30 [Available from: <https://www.statista.com/statistics/489131/share-of-renewables-in-power-generation-globally/>].
- [5] McEvoy A, Markvart T, Castañer L, Markvart T, Castaner L. **Practical handbook of photovoltaics: fundamentals and applications**: Elsevier; 2003. Number of.
- [6] Shah AV. **Thin-film silicon solar cells**: EPFL press; 2010. Number of.
- [7] Lima RCd. **Development of Thin Film Silicon Tandem Solar Cells in 3 Terminal Configuration**: Hanze University of Applied Sciences, Groningen; 2016.
- [8] GmbH Ve. **WACOM WXS-90S-L2 AM1.5GMM [cited 2018 14 August]**. Available from: <https://vosselectronic.de/34-solar-simulator/58-wacom-solar-simulator-two-lamp-type>.

[9] Khan F, Singh S, Husain M. **Effect of illumination intensity on cell parameters of a silicon solar cell**. *Solar Energy Materials and Solar Cells*. 2010;94(9):1473-6.

[10] PerkinElmer. **LAMBDA 950 UV/Vis Spectrophotometer** [Available from: <http://www.perkinelmer.com/product/lambda-950-uv-vis-nir-spectrophotometer-1950>].

[11] Abou-Ras D, Kirchartz T, Rau U. **Advanced characterization techniques for thin film solar cells**: John Wiley & Sons; 2016. Number of.

[12] Reetz W, Kirchartz T, Lambertz A, Hüpkes J, Gerber A, editors. **Current–voltage and spectral response based characterization of thin film silicon solar cells—investigation of primary error sources**. 24th Eur Photovolt Sol Energy Conf, WIP Renewable Energies, Munich, Germany, Hamburg, Germany; 2009.

[13] Sandbaumhüter F, Agbo SN, Tsai C-L, Astakhov O, Uhlenbruck S, Rau U, et al. *Compatibility study towards monolithic self-charging power unit based on all-solid thin-film solar module and battery*. *Journal of Power Sources*. 2017;365:303-7.

[14] Agbo S, Merdzhanova T, Rau U, Astakhov O. **Illumination intensity and spectrum-dependent performance of thin-film silicon single and multijunction solar cells**. *Solar Energy Materials and Solar Cells*. 2017;159:427-34.

جامعة النجاح الوطنية

كلية الدراسات العليا

أنظمة الخلايا الكهروضوئية المتجانسة المتصلة بالبطاريات كوسيلة لتوليد
كهربائي مستدام

أعداد

محمد وليد محمد جابر

إشراف

د. تامر خطيب

قدمت هذه الأطروحة استكمالاً لمتطلبات الحصول على درجة الماجستير في هندسة الطاقة
النظيفة وترشيد الاستهلاك، بكلية الدراسات العليا، في جامعة النجاح الوطنية، نابلس - فلسطين.

2019

ب

أنظمة الخلايا الكهروضوئية المتجانسة المتصلة بالبطاريات كوسيلة لتوليد كهربائي مستدام

إعداد

محمد وليد محمد جابر

إشراف

د. تامر خطيب

الملخص

تعد أزمة الطاقة العالمية وطرق توفير طاقة متجددة نظيفة لتوفير الاستدامة من أهم ما يشغل المجتمع العلمي، حيث تعتبر الطاقة الشمسية أحد الحلول المتصدرة لهذه الأزمة، وتعد رفع كفاءة الخلايا الشمسية وطرق تخزين الطاقة منها من أكثر المواضيع أهمية، حيث سُجلت أعلى كفاءة لخلايا شمسية وصلت إلى 26.6% في وقته. وبعد إيجاد طريقة تخزين فعالة لطاقة من الخلايا الشمسية تضمن توفير الطاقة في فترات انعدام مصدر الضوء من أهم التحديات، وتعتبر البطاريات الصلبة من أهم طرق تخزين الطاقة الكهربائية وإعادة استخدامها بفعالية عالية، وعن طريق دمج هاذين المكونين مع بعضهم البعض للحصول على نظام متكامل لخلايا ضوئية وبطارية يمكن تقديم تصميم متكامل لنموذج خلية شمسة وبطارية مدمجة. هذه الدراسة ستوفر عرض دقيق لمراحل تصميم جزء الخلية الشمسية لنظام المتكامل المقترح، وتصميم خلية شمسية ثلاثية الأطراف/ ثلاثية الوصلات، الطبقة العليا مكونة من (a-Si:H) والطبقة سفلى ترادفية مكونة من ($\mu\text{c-Si:H}/\mu\text{c-Si:H}$)، بترتيب وصلات (p-i-n/n-i-p/n-i-p) على الترتيب، وتحقيق الدراسة أقصى تطابق في الجهد الكهربائي بين الطبقتين يصل إلى (95.67%). ودراسة الاستجابة الطيفية لهذه الخلية تحت مصادر ضوء مختلفة (AM1.5, LED, tube, halogen) ومستويات أضواء مختلفة (1sun) إلى (0.0000194sun)، ورصد ودراسة معاملات الخلية (V_{oc} , I_{sc} , FF, η) وعلاقتها باختلاف مصادر الضوء ومستويات الإضاءة، وتحليل سلوك الضوء خلال الخلية وتحديد المعاملات المسببة للخسائر الضوئية. وبعد ذلك مقارنة سلوك التصميم المقترح مع مجموعة من الخلايا الشمسية (2T-device, Perovskite, SHJ)، وفي المرحلة الأخيرة، التحقق من قدرة التصميم المقترح على شحن نموذج بطارية تجارية (3.7V135mAh)، والذي سجل كفاءة

ج

تحويل الطاقة الشمسية لشحن تصل في معدلها إلى (10%) تحت مصدر ضوء من نوع (AM1.5).